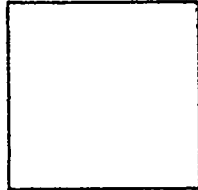


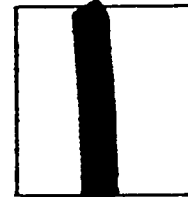
PHOTOGRAPH THIS SHEET

AD-A951 872

DTIC ACCESSION NUMBER



LEVEL



INVENTORY

Tech Rept. No. 9

DOCUMENT IDENTIFICATION

Contract W33-038-AC-16697

15 Apr. 49

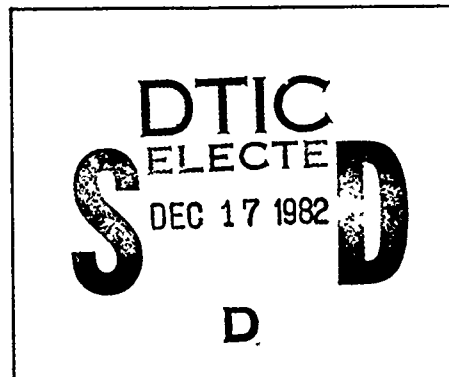
DISTRIBUTION STATEMENT A

Approved for public release;
Distribution Unlimited

DISTRIBUTION STATEMENT

ACCESSION FOR	
NTIS	GRA&I <input checked="" type="checkbox"/>
DTIC	TAB <input type="checkbox"/>
UNANNOUNCED	<input type="checkbox"/>
JUSTIFICATION	
(15 Apr. 1949)	
BY	
DISTRIBUTION /	
AVAILABILITY CODES	
DIST	AVAIL AND/OR SPECIAL
A	

Released



DATE ACCESSIONED

DISTRIBUTION STAMP

UNANNOUNCED

82 12 17 009

DATE RECEIVED IN DTIC

PHOTOGRAPH THIS SHEET AND RETURN TO DTIC-DDA-2

AD A 951872

ASIAC

407

A LIMITED INVESTIGATION OF THE
BENDING OF 24S-T ALUMINUM ALLOY ANGLE BEAMS
IN THE PLASTIC RANGE

BY

BRUCE G. WOOLPERT
H. NORMAN ABRAMSON
HARRY A. WILLIAMS

TECHNICAL REPORT NO. 9

AIR FORCES CONTRACT W33-038 AC-16697

DEPARTMENT OF CIVIL ENGINEERING
STANFORD UNIVERSITY
STANFORD, CALIFORNIA

APRIL 15, 1949

DISTRIBUTION STATEMENT
Approved for public release
Distribution Unlimited

A LIMITED INVESTIGATION OF THE BENDING OF
24S-T ALUMINUM ALLOY ANGLE BEAMS IN THE ELASTIC RANGE

By

Bruce G. Woolpert, H. Norman Abramson
and Harry A. Williams

Technical Report No. 9

Air Forces Contract W33-038 Ac-16697

Civil Engineering Department
Stanford University
Stanford, California

April 15, 1949

ABSTRACT

An earlier investigation revealed the necessity for further study of the bending of unsymmetrical beams in the plastic range, inasmuch as twist occurs and has a marked effect.

Angle cross-section beams of aluminum alloy 24 ST material were subjected to bending in the plastic range with the planes of loading at angles of 0° , 30° , 60° , and $76^\circ-07'$ to the minor principal axis of the cross-section. The moment was applied by means of an eccentric load, with a relatively long moment arm.

For a simplified approach, it was found that Cozzone's method of plastic bending analysis and an analysis based on an exponential relationship between stress and strain both gave reasonable correlation between theoretical and experimental bending moments in the plastic range beyond the yield strength. Both methods are approximate since they assume that the neutral axis does not rotate or translate and the cross-section does not rotate. The exponential method is not valid in the range below the yield strength.

Other factors concerned with the general behavior of angle beams subjected to plastic bending are also considered.

INTRODUCTION

Pure bending in the plastic range when the applied loads are parallel to a principal plane of bending has been studied by a number of investigators (references 1 to 6). When the loads are not parallel to a principal plane, the complexity of the problem increases many fold. The complexity is further increased when the beam cross-section is not symmetrical with respect to a principal axis. Goodier's general solution of the problem for open sections, (reference 9), indicates the difficulties encountered even under elastic conditions. It is seen at once that pure bending, as it is usually understood, does not prevail except under very restricted conditions.* If the applied torsion and axial thrust are eliminated from Goodier's solution, it is evident that a torsion couple must still act at any cross-section except the mid-point of the length unless all of the deflection is parallel to a principal plane. This couple produces twist and it is evident that the relationship between components causing normal stress must vary along the length of the beam. Hence, the neutral axis must rotate also.

If plastic action prevails to any large extent, the various parts of an open section must be relatively heavy and the usual assumptions for shear flow might be questioned. The major obstacle to the solution of the plastic bending problem results, however, from the non-linear relationship between stress and strain. This leads to even more complex relationships between moment and stress and eliminates the use of superposition. Except in special cases, pronounced curvature results in considerable rotation.

It is evident that a rigorous solution of the problem of plastic bending of unsymmetrical beams must be developed from the concepts of pure plasticity.

*This general subject is discussed further in reference 11.

Phillips presents the exact theory of combined pure bending and axial force for a prismatical bar using the equations of the theory of plastic deformations. The solution of the differential equations is extremely difficult. Hence, it appears wise, for the benefit of the designer, to seek approximate but practical solutions which will give reasonably accurate results.

In a previous investigation, by one of the authors (reference 7), of plastic bending when loads were not parallel to a principal plane, some exploratory tests of angle beams were made. A modification of Cozzone's approach (reference 5) gave a resisting moment at the mid-span which was less than 15 per cent larger than the applied end moment until plastic instability occurred at which time the per cent difference increased rapidly. These experiments were made with 1/4" by 1" by 2" angle beams of 75 S-0 aluminum alloy with an 8" clear span. Tests were made with the plane of loading at various angles from 0° to 90° with the 2" leg.

The present investigation is an extension of the previous work and is confined to angle beams of the same cross-section. In planning the program it was decided to increase the clear span to 24" in order to accentuate rotation and to apply the end moments by means of a small eccentric load with a relatively large moment arm.* The primary purpose is to determine to what extent a relationship between bending moment at the mid-span and outer fiber stress will agree with the applied end moment if a simplified theoretical approach is used in the analysis. Hence, the resisting moment is computed by a modification of Cozzone's graphical method used in reference 5 and by an analytical method based on an exponential relationship between stress and strain. Both methods neglect rotation and other variables in the interests of simplicity. Data on rotation of the cross-section and movement of the neutral axis are also presented to add information regarding the general behavior of the tested beams.

*As used in this report, rotation refers to twist and not to changes in end slope of the longitudinal axis.

NOTATION

- a constant dependent upon the material for the exponential equation
 a_c distance to point on neutral axis, inches
 Δa_c change in a_c , inches
 b length of short leg, inches
 c general symbol for distances from neutral axis, inches
 c_c, c_t distance from neutral axis to outer compressive and tensile fibers, respectively, inches
 d, g symbols for particular cross-section dimensions, inches
 e general symbol for strain, inches per inch
 e_c, e_t outer fiber compressive and tensile strain, respectively, inches per inch
 e_1 to e_{12} strains determined experimentally, inches per inch
 f_c, f_t stress determined from compression and tension tests, respectively, psi
 f_p, f_y proportion limit stress and yield strength, respectively, from average stress strain curve, psi
 f_m outer fiber bending stress, psi
 f_{mc}, f_{mt} outer fiber compressive and tensile stress, respectively, psi
 f_o Coszone's intercept stress, psi
 f_{oc}, f_{ot} intercept stress for compressive and tensile area, respectively, psi
 k_c, k_t Coszone's beam section constants
 K constant in exponential equation, psi
 x_n, y_n distance to point on rotated neutral axis, inches
 E Young's modulus of elasticity, psi
 I_x, I_y, I_{xy} moments and product of inertia of cross-section with respect to x and y axes, inches⁴

- $I_X I_Y$ moment of inertia with respect to principal axis, inches⁴
 $I_{N_c} I_{N_t}$ moment of inertia of compressive and tensile areas, respectively,
 with respect to neutral axis, inches⁴
 K_f plastic stress function based on average stress-strain curve, psi
 K_{fc}, K_{ft} plastic stress function based on compression and tensile stress-strain
 curves, respectively, psi
 L moment arm to centroid at mid-span, inches
 M_e experimental bending moment, inch-pounds
 M_{th} bending moment computed analytically, inch-pounds
 M_{th}^c, M_{th}^t bending moments computed analytically for compressive and tensile
 areas, respectively, inch-pounds
 n power to which e and ρ are raised in the exponential equation
 P dynamometer load, pounds
 Q_{mc}, Q_{mt} statical moment of compressive and tensile areas, respectively, inches³
 r distance from neutral axis to an element in the beam cross-section used
 in the derivation of the exponential equation, inches
 t thickness of angle beam leg, inches
 ΔT_c $\Delta a_c \sin \gamma$, inches
 α angle between principal axis and neutral axis, degrees
 $\Delta \alpha$ change in angle α , degrees
 θ angle between plane of loading and y axis, degrees
 ϕ angle between plane of loading and normal to neutral axis, degrees
 ρ radius of curvature, inches
 γ angle between x -axis and neutral axis, degrees

TEST SPECIMENS AND APPARATUS

Test Specimens and Stress-Strain Characteristics

The test specimens were machined to the dimensions shown in Fig. 1 from two ten-foot long 24 S-T aluminum alloy bars. These bars were 1 by 2 inches in cross-section and were designated bars M and N. Photographs of the specimens after testing are shown in Fig. 2.

Considerable difference between the stress-strain curves in tension and compression exists for 24 S-T aluminum alloy, but inasmuch as this material is commonly used in practice, it was decided to use it rather than some other material which might have tension and compression curves that are in better agreement. All analytical computations were based upon an average stress-strain curve. Tension and compression samples from a number of bars, including M and N, gave stress-strain data as indicated in Figs. 3 and 4. The curves of Fig. 5 were selected as being representative of the material in bars M and N and were used for all computations.

Three tension and three compression specimens were taken from each end of several bars of the single shipment. The tension specimens were 8 inches long over all and were machined to 1/8 inch by 1/2 inch at the reduced section. The compression specimens were 15/16 inch by 1 inch by 3 inches in length and might be referred to as the block type of compression specimen.

Loading Apparatus

The arrangement of the loading apparatus used for bending the angle beams is shown in Figs. 6 and 7. The two lever arms machined from 3/4 inch steel plate were supported at one end by cables from an overhead beam and at the other end by ball bearing rollers.

Tracks for the rollers were attached to a heavy table immediately below the suspended arms and so arranged as to constrain the movement of the fore-end of the arms in a path perpendicular to the center line of the apparatus.

The arms at the cable end were provided with fittings which securely held the specimen in a position perpendicular to the two arms and parallel to the tracks, thus forming a rigid frame. The specimen fittings were further designed, by means of a movable disk which could be secured with a retaining ring, so that the specimen could be rotated about its lengthwise axis to provide any angle of bending desired. The load was applied through cables attached to the arms as shown. It is obvious from the loading arrangement that pure bending was only approximated, due to the presence of a slight axial load.

Strain Apparatus

Strain readings were taken with an SR-4 type indicator which is shown to the left of the bending apparatus in Fig. 6. The strains were measured at various points around the center cross-section by SR-4 type A-12 electrical strain gages cemented to the specimen. A typical arrangement of strain gages around the center cross-section is shown in Fig. 8.

TEST PROCEDURE

Each specimen was measured with a micrometer and electric strain gages were cemented to the specimen along previously scribed lines. The specimen was then placed in the bending apparatus and carefully adjusted to the desired angle of rotation. A preliminary check on the operation of the entire system was then made by bending the beam until the maximum stress was approximately two-thirds of the proportional limit and reducing the recorded data to confirm the proper operation of all components of the system.

The normal testing procedure was to apply an increment of load, stop the testing machine, and immediately record the strain indicator readings for all gages. The latter step was particularly important in the plastic range because of creep.

As the plastic range was reached, the curvature of the beam decreased the moment arm. This decrease was measured by means of a plumb bob attached near the centroid of the beam and hanging along side a scale measuring to the nearest 0.02 inch.

Specimens were removed when the reduction in moment arm was sufficient to tend to prevent any increase in bending moment when additional load was applied. Generally, one or more of the electric strain gages had become inoperative at this point, and the maximum outer fiber strain was on the order of 2 per cent.

Rotations were measured by means of an arm attached near the beam centroid. A protractor and plumb bob at the end of this arm enabled the rotations to be read directly to the nearest 0.2 degree.

ANALYTICAL PROCEDURE

Cozzone's Method

From reference 7, Cozzone's method, as proposed in reference 5, may be modified for an angle beam if the rotation of the beam in the plastic range is neglected and the neutral axis is assumed to remain stationary. Neglecting these factors, an approximate solution may be made by dividing the cross-section into a compression area and a tension area. The resisting moment of the compression area is obtained by assuming the symmetrical cross-section shown in Fig. 1(b). The resisting moment of this beam is computed and divided by two. This is equivalent to computing I_{N_c} for one-half the cross-section only. Then $k_c = \frac{y_{mc}}{I_{N_c}/c_c}$ and the moment becomes

$$M'_{th} = \frac{I_{N_c}}{c_c} \frac{1}{\cos \theta} \left[f_{mc} + f_{oc} (k_c - 1) \right] \quad (1)$$

A similar approach for the tension area (Fig. 1(c)) results in the equation

$$M''_{th} = \frac{I_{N_t}}{c_t} \frac{1}{\cos \theta} \left[f_{mt} + f_{ot} (k_c - 1) \right] \quad (2)$$

The final restraining moment is

$$M_{th} = M'_{th} + M''_{th} \quad (3)$$

The relationship between stress, strain, and intercept stress (f_o) based on an average stress-strain curve is presented in Fig. 5.

Exponential Method

An exponential relationship between stress and strain may be formulated which will closely approximate the stress-strain curve in the range of higher strains. This relationship takes the form

$$f\epsilon = ae^n - K \quad (4)$$

But it must be noted that when stress equals zero, strain is not zero although it may be approached through proper selection of the constant K .

If $\epsilon = \frac{r}{\rho}$ then equation (4) becomes

$$f = \frac{ar^{n-1}}{\rho^{n-1}} - \frac{K\rho}{r} \quad (5)$$

In the case of angle beams, an expression for bending moment may be found as follows:

$$M_{th} = \frac{l}{\cos \beta} \left[\frac{a}{\rho^{n-1}} \frac{1}{(n+1)(n+2)} \left(d c_u^{n+1} - g c_s^{n+1} \right) - \frac{K\rho}{2} (d c_u - g c_s) \right. \\ \left. + \frac{tc_3}{\cos \gamma} \left(\frac{a}{\rho^{n-1}} \frac{c_3^n}{n+1} - K\rho \right) + \frac{tc_4}{\sin \gamma} \left(\frac{a}{\rho^{n-1}} \frac{c_4^n}{(n+1)} - K\rho \right) \right] \quad (6)$$

where all notation is referred to Fig. 9. A rather complete derivation of equation (6) may be found in the appendix.

Comparison of Bending Moments

It is easier to compare experimental and computed bending moments in the plastic range than to compare outer fiber stresses; hence, the general procedure of this report has been to take the experimental strain corresponding to a given load, determine the necessary stress values from a representative stress-strain curve and then insert these in the appropriate formula to compute the so-called theoretical bending moment.

The ratio of M_{th}/M_t has been taken as the criterion for comparison of bending moments.

RESULTS AND DISCUSSION

In order to avoid needless repetition, it was decided to present detailed information on a single typical angle beam, namely M-4, $\theta = 0^\circ$, and to present only the important test results for the remainder of the specimens tested.

Angle beam M-1 has been omitted from this report inasmuch as its purpose was only to provide a check on the reliability of the bending and strain measuring apparatus.

Strain Measurements

Typical load and strain data are presented in table 3, where the particular strain gage locations are shown in Fig. 8(b).

In general strain readings agreed reasonably well for two specimens tested under the same conditions. With some exceptions, the difference was not more than 5 per cent in the elastic range and 10 per cent in the plastic range. The latter might be partially explained by the non-uniformity of the material itself and by the difficulty in locating SR-4 gages exactly the same on duplicate specimens. Such discrepancies, however, did not greatly affect the computed bending moment because even large differences in outer fiber strain did not affect the stress values when working on the higher range of the stress-strain curve, where the slope is small.

Maximum Strains and Neutral Axis Locations

Maximum compressive strain (e_c), maximum tensile strain (e_t), location of neutral axis intersection with the outside of the short leg (x_n), and location of neutral axis intersection with the outside of the long leg (y_n) were all found by a graphical method which assumes a linear variation of strain across

each face of the beam. A sample solution illustrating the method is given in Fig. 10. The procedure was to lay out to scale a leg of the beam with proper gage locations and for a given load plot the strains for each gage perpendicular to the leg. A straight line connecting all strains for a particular bending moment was drawn, from which e_c (or e_t) and x_n (or y_n) could be read directly. Tables 1, 2, 4, 6, 7, and 8 present this data for all beams.

One would expect the outer fiber strains to become less exact when determined as described above as the rotation and warping increases. However, such errors would have little effect on bending moment in the plastic range.

The x_n and y_n values are approximations only because these distances are quite sensitive to small change in strain. When a gage was near the neutral axis and the strains were relatively small, the effect of errors in the strain was quite pronounced. However, the results when considered collectively indicate definite trends.

Theoretical Vs Experimental Bending Moments

Theoretical bending moments were computed from equations (3) and (6). The per cent differences between theoretical and experimental bending moments were computed from the expression $(M_{th}/M_t - 1) \times 100$ per cent. A computation table for theoretical bending moment by both Cozzone's method and the exponential method is presented for a typical angle beam in table 4. Tables 1 and 2 and 5 through 8 present the values of M_{th} by both methods for all beams, as well as the equation used. These values are presented graphically in Figs. 11 through 13. For comparative purposes, results for different angles of loading are shown on the same figures. The elastic, partially-elastic, and plastic ranges are shown on these graphs by indicating on the moment scale the

approximate values of the experimental moment at which the proportional limit, f_p , and the 0.2 per cent offset yield strength, f_y , were reached in the outer fibers of the beam in question.

An inspection of Figs. 11 through 13 shows that the theoretical bending moment was generally within approximately 10 per cent of the experimental moment in the plastic range beyond the yield strength for both Cozzone's method and the exponential method. The differences in the range below the yield strength were approximately the same for Cozzone's method but very much greater for the exponential method, which is to be expected in view of the fact that the exponential relationship between stress and strain should not be used below the yield strength. In certain cases where the twist was large, the differences were slightly greater.

It will be noted that the maximum applied moment is larger for one beam than for the other at both the 0° and 30° positions. However, the difference is only about 7 per cent which might be explained by a difference in the materials and by the difficulty in exactly duplicating test procedure.

Beam M-5 which was tested at 60° gave results consistent with other specimens. It is seen from Fig. 1 that the neutral axis makes an angle of less than 2° with the principal axis. There was little rotation of the cross-section. It was then decided to test beam N-7 in such a position that the neutral axis coincided with the principal axis. The results showed negligible rotation of the cross-section although the rotation and translation of the neutral axis were consistent with other specimens. However, the difference between the computed and experimental bending moment appears out of line with the results for the 60° beam, M-5. Since there was insufficient time to repeat the experiment, no explanation can be offered for the discrepancy.

Change in Position of the Neutral Axis

Figures 14 through 16 show the rotation and translation of the neutral axis for the various beams. The values of $\Delta\alpha$ and ΔT_c may be computed from the expressions

$$\Delta\alpha = (90^\circ - \alpha) - \tan^{-1} \left(\frac{x_n}{y_n} \right) + 13^\circ 58' \quad (7)$$

$$\Delta a_c = 0.261 + 0.760 \frac{x_n}{y_n} - x_n \quad (8)$$

$$\Delta T_c = \Delta a_c \sin (\alpha - 13^\circ 58') \quad (9)$$

These expressions are derived from simple geometrical relationships, referred to Fig. 1. The angle $\Delta\alpha$ is considered positive when the neutral axis rotates clockwise. Δa_c is positive if it represents an increase in a_c . When $\Delta T_c = \Delta a_c \sin \alpha$ is positive, it indicates that the neutral axis is translating toward the compression side of the beam. It should be noted that all of these changes are with respect to the axes of the cross-section. Obviously they are intimately related to the cross-section rotation as will be discussed in the next section.

In general, rotations were all counterclockwise and were of the order of magnitude of 3 to 4 degrees for all beams. The translations were all positive and of an order of magnitude of 0.01 inches except for angle beam N-7 which was approximately 0.02 inches.

The same information is presented in another manner in Figs. 17 through 19 by plotting the values of x_n and y_n against applied moment. Since x_n and y_n were obtained by graphical methods, the values are approximate only.

Curves have been indicated to show general trends. When the curves move in the same direction, translation is indicated; when they move in opposite directions and cross over, rotation is indicated.

Behavior of Resisting Couple at Mid-Span as Cross-Section Rotates

The torsion couple which causes the beam to rotate must be equal to zero at the mid-span because of symmetry. Hence, the only couple acting at this section is the conventional bending moment couple. Also, equilibrium conditions demand that it be equal in magnitude and opposite in direction to the external couple. It must also lie in a plane which is parallel to that of the latter.

The location of the resisting couple for beam M-4 is shown in Fig. 20 for three stages of loading. The resultant tensile and compressive forces are F_t and F_c , respectively, and are located approximately to scale. The forces were evaluated and located by graphical integration. The difference in magnitudes was as follows:

Fig. 20	External Moment (in-kips)	F_t (kips)	F_c (kips)	Arm (inches)	Resisting Couple (in-kips)
(a)	6.21	5.0	4.7	1.24	5.52
(b)	11.90	10.3	10.6	1.00	10.45
(c)	13.03	13.7	13.2	0.86	11.55

It is seen that the percentage difference remains essentially constant with increasing load. Some error is introduced by the graphical solution, and also by the fact that the true external moment couple does not remain in a horizontal plane but rotates slightly as the beam deflects vertically. Hence, its magnitude becomes increasingly larger than PL and the rotation

is counterclockwise in Fig. 20. It will be noted that the resisting couple rotates in the same direction.

The sketches of Fig. 20 also show that the neutral axis rotates considerably less, with respect to the cross-section, than the latter rotates with respect to its original position. This difference depends on the shape of the cross-section and on the degree of plasticity. In this case, when the left hand tip of the tension leg becomes stressed beyond the proportional limit, a "softening" results and the resultant, F_t , moves toward the neutral axis and away from the "soft" area. When the stress at the outer compressive corner moves into the plastic range, a similar shift is made by F_c . Since the resisting couple must remain parallel to the plane of the external couple, the neutral axis rotation must be adjusted with the cross-section rotation so that the stress distribution satisfies equilibrium conditions.

Deviation From Pure Bending

As mentioned earlier, the bending apparatus used only roughly approximated pure bending. Actually, an axial stress having a maximum value of approximately 1000 p.s.i. existed. Quite often in practice combined loadings of this type are encountered; therefore, the investigation of this report more nearly approaches practical applications. In contrast, a rigid method of analysis for the loading used is considerably more difficult than for pure bending. However, it has been shown that an analysis which assumes pure bending gave fairly consistent results none the less. Since rotation was neglected, the agreement resulted to a certain extent from the fact that errors were partially compensating and moment was not particularly sensitive to strain variations in the plastic range.

As a matter of interest, strain gages were placed on beam M-5 as shown in Fig. 8(a). The results are shown in table no. 6 where it will be noted that the moment arm has been corrected for the different degrees of curvature existing at stations B and C.

Inspection of the data shows that strains were essentially constant at the three stations. This is partially accounted for by the fact that while the resultant moment couple increased from A to C, the bending couple about the neutral axis remained approximately constant after the torsion component was subtracted. However, the x_n and y_n values show that the neutral axis location was different at each station as might be expected.

CONCLUSIONS

Since rotation of the beam cross-section and of the neutral axis were neglected in the analysis, any conclusion must be confined to the particular beam shape used in the experiments. If the analysis is extended to shapes having essentially different proportions from the one reported in this investigation, the differences between a theoretically computed bending moment and the actual moment might easily be several times as large as those reported. This statement also applies if another type of loading is used. The method should be extended to other material with caution.

The following conclusions can be drawn from the results of this particular investigation:

1. A modification of Cozzone's method of plastic bending analysis gave approximate but reasonable results. For the particular material and configuration investigated, the correlation between computed and experimental bending moments in the semi-plastic and plastic ranges was within 10 per cent.
2. An exponential relationship between stress and strain also gave reasonable results. For the particular material investigated, the correlation between computed and experimental bending moments in the plastic range beyond the yield strength was within 10 per cent. The method is not valid for the range below the yield strength. Simplification of the method appears to be possible, but required further study.
3. Rotation of the cross-section was the primary factor limiting the ultimate strength of the beams. This rotation cannot be included in a simplified analysis such as was used in this investigation.

4. It is suggested that if further investigations of the general problem of this report are to be carried out, a larger testing machine be used in order to carry the tests as far into the plastic range as possible. Further suggestions are: (1) an apparatus for providing a more nearly pure bending condition than the apparatus of this report be used, and (2) that rectangular specimens be used with test sections machined to provide a variety of cross-section shapes and proportions, as well as lengths of test sections.

REFERENCES

1. Timoshenko, S., "Strength of Materials," Part II, 2nd Edition, Chapt. VIII; D. Van Nostrand Co., Inc., New York, 1941.
2. Bellschmidt, J. I., "The Stresses Developed in Sections Subjected to Bending Moment," Journal of the Royal Aeronautical Society, Vol. XLVI, No. 379, July 1942, pages 161-182.
3. Osgood, W. R., "Plastic Bending," Jour. Aero. Sciences, Vol. 11, No. 3, July 1943, Page 213.
4. Rappleyea, F. A. and Eastman, E. J., "Flexural Strength in the Plastic Range of Rectangular Magnesium Extrusions," presented at the 12th Annual Meeting of Inst. of the Aero. Sciences, New York, January 1944.
5. Cozzona, F. P., "Bending Strength in the Plastic Range," Jour. Aero Sciences, Vol. 10, No. 5, P. 137, May 1943.
6. Williams, H. A., "Pure Bending in the Plastic Range," Jour. Aero. Sciences, Vol. 14, No. 8, P. 457, August 1947.
7. Williams, H. A., "An Investigation of Pure Bending in the Plastic Range When Loads Are Not Parallel to a Principal Plane," (Performed under contract to the N.A.C.A.; as yet unpublished.)
8. Goodier, J. N., "The Buckling of Compressed Bars by Torsion and Flexure," Cornell University Experiment Station, Bull. No. 27, December 1941.
9. Goodier, J. N., "Flexural-Torsional Buckling of Bars of Open Section Under Bending, Eccentric Thrust or Torsional Loads," Cornell University Experiment Station, Bull. No. 28, January 1942.
10. Davis, D. S., "Empirical Equations and Nomography," 1st Edition; McGraw-Hill Book Co., Inc., New York, 1943, Pages 11-14.

11. Williams, H. W., "Stability of Rectangular and I Section Beams in the Plastic Range", Technical Report No. 8, Air Forces Contract W33-038 Ac-16697, June 1, 1949.
12. Phillips, A., "Pure Bending with Axial Force in the Theory of Plastic Deformations", Stanford University Technical Report No. 3, January 1949.

APPENDIXDerivation of the Exponential Equation for Theoretical Bending Moment of an Angle Beam

A number of equations relating stress to strain beyond the proportional limit have been suggested. Several of these were investigated by the authors with the view of developing a suitable flexure formula for an angle cross-section. Many of the expressions lend themselves quite readily to a simple formula for a rectangular beam with loads in a principal plane but become quite complicated for more general solutions.

It was noticed that when the product fe was plotted against e for a number of materials, the outer portion of the curve was of the form

$$fe = ae^n$$

It was noticed further that this expression could be modified by conventional methods (reference 10) so that it also roughly approximated the straight line portion of the stress-strain curve by writing it in the form

$$fe = ae^n - K$$

or

$$f = ae^{n-1} - K/e \quad (1)$$

It is evident that this curve does not pass through the origin when $e = 0$; however, K can be adjusted so that it passes quite close to the origin. Using this equation as a basis, approximate expressions can be derived for an angle beam.

If no warping of cross-sections occurs (all notation referred to Fig. 9)

$$a = \frac{r}{\rho}$$

and

$$f = \frac{ar^{n-1}}{\rho^{n-1}} - \frac{K_0}{r} \quad (2)$$

Considering the area above the neutral axis, i.e. the compression area:

$$\begin{aligned}
 \text{Outer triangle: } M_{\Delta}^I &= \int f r s d r \quad \text{where } \frac{s}{d} = \frac{c_u - r}{c_u} \\
 &= \int_0^{c_u} \left(\frac{a r^n}{\rho^{n-1}} - \frac{K \rho}{r} \right) r \left(1 - \frac{r}{c_u} \right) d r \\
 &= d \left[\frac{a c_u^{n+1}}{\rho^{n-1}} \left(\frac{1}{(n+1)(n+2)} - \frac{K \rho c_u}{2} \right) \right] \quad (3)
 \end{aligned}$$

$$\text{Inner triangle: } M_{\Delta}^{II} = g \left[\frac{a c_s^{n+1}}{\rho^{n-1}} \left(\frac{1}{(n+1)(n+2)} - \frac{K \rho c_s}{2} \right) \right] \quad (4)$$

$$\text{and } M_{\Delta} = M_{\Delta}^I - M_{\Delta}^{II}$$

$$= \frac{a}{\rho^{n-1}} \frac{1}{(n+1)(n+2)} \left(d c_u^{n+1} - g c_s^{n+1} \right) - \frac{K \rho}{2} \left(d c_u - g c_s \right) \quad (5)$$

Considering the area below the neutral axis, i.e. the tension area:

$$\begin{aligned}
 \text{h - leg: } M_h &= \int f r s d r \\
 &= \int_0^{c_3} \left(\frac{a r^{n-1}}{\rho^{n-1}} - \frac{K \rho}{r} \right) r \frac{t}{\cos \gamma} d r \\
 &= \frac{t}{\cos \gamma} \left(\frac{a}{\rho^{n-1}} \frac{c_3^{n+1}}{n+1} - K \rho c_3 \right) \quad (6)
 \end{aligned}$$

$$\text{b - leg: } M_b = \frac{t}{\sin \gamma} \left(\frac{a}{\rho^{n-1}} \frac{c_u^{n+1}}{n+1} - K \rho c_u \right) \quad (7)$$

The total resisting moment is the sum of equations (5), (6) and (7) or

$$\begin{aligned}
 M_{th} &= \frac{1}{\cos \phi} \left[\frac{a}{\rho^{n-1}} \frac{1}{(n+1)(n+2)} \left(d c_u^{n+1} - g c_s^{n+1} \right) - \frac{K \rho}{2} \left(d c_u - g c_s \right) + \right. \\
 &\quad \left. \frac{t c_3}{\cos \gamma} \left(\frac{a}{\rho^{n-1}} \frac{c_3^n}{n+1} - K \rho \right) + \frac{t c_u}{\sin \gamma} \left(\frac{a}{\rho^{n-1}} \frac{c_u^n}{n+1} - K \rho \right) \right] \quad (8)
 \end{aligned}$$

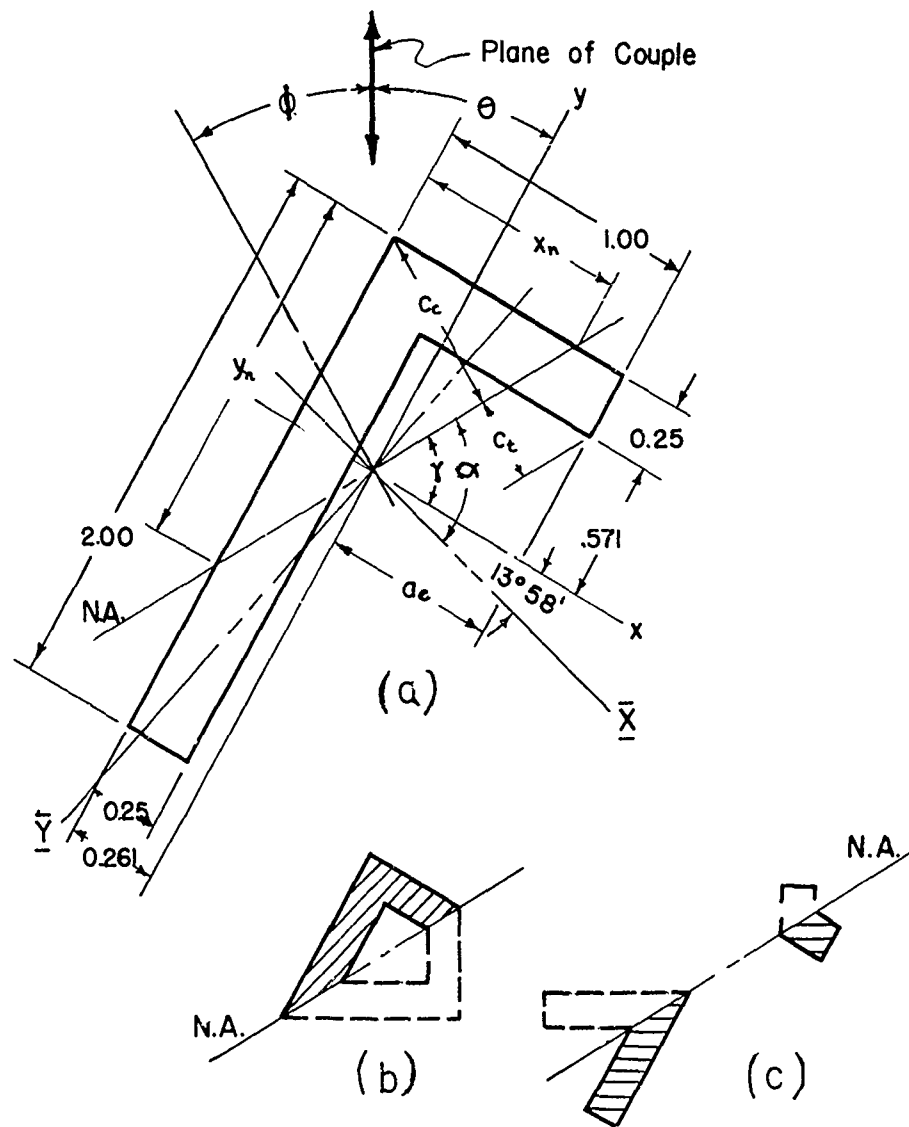
Discussion of the Exponential Method

Figure 21 presents curves which may be used for rapidly determining values of ρ^{n-1} , c^n , and c^{n+1} for known values of ρ and c . Although this figure is limited to aluminum alloy 24 S-T material and a particular value of n , it is relatively simple to construct similar figures for other materials after the proper values for n and K have been determined.

Values of n and K for materials similar to the one of the present investigation are not difficult to determine, by the method of reference 10, when applied to the stress-strain curve of the material in question.

An exploratory investigation aimed at simplifying the exponential method would appear to indicate that for the portion of the stress-strain curve beyond the yield strength, equation (8) may be modified by setting $K = 0$. The effect is to increase slightly the value of the computed bending moment. * Again, such a generality applies only to the particular conditions of this report.

*Inasmuch as the unmodified exponential equation (eq. 8) usually gives values for the computed bending moment which are less than the experimental moment, the modification just mentioned would apparently tend to bring the computed and experimental moments into closer agreement.



SECTION PROPERTIES								
Rectangular Axes				Principal Axes				
$I_x = 0.2706$				$I_{\bar{x}} = 0.2554$				
$I_y = 0.0456$				$I_{\bar{y}} = 0.0308$				
$I_{xy} = 0.0600$								
θ	α	ϕ	I_e	I_t	Q_{mc}	Q_{mt}	C_e	C_t
0°	66°33'	52°35'	0.0330	0.0385	0.0929	0.0862	0.670	0.744
30°	83°37'	39°39'	0.0167	0.0173	0.0635	0.0622	0.507	0.518
60°	88°13'	14°15'	0.0140	0.0177	0.0581	0.0558	0.457	0.572
76° 07'	90°00'	-0° 07'	0.0127	0.0183	0.0570	0.0537	0.434	0.592

FIG. 1 — ANGLE BEAM CROSS SECTION PROPERTIES

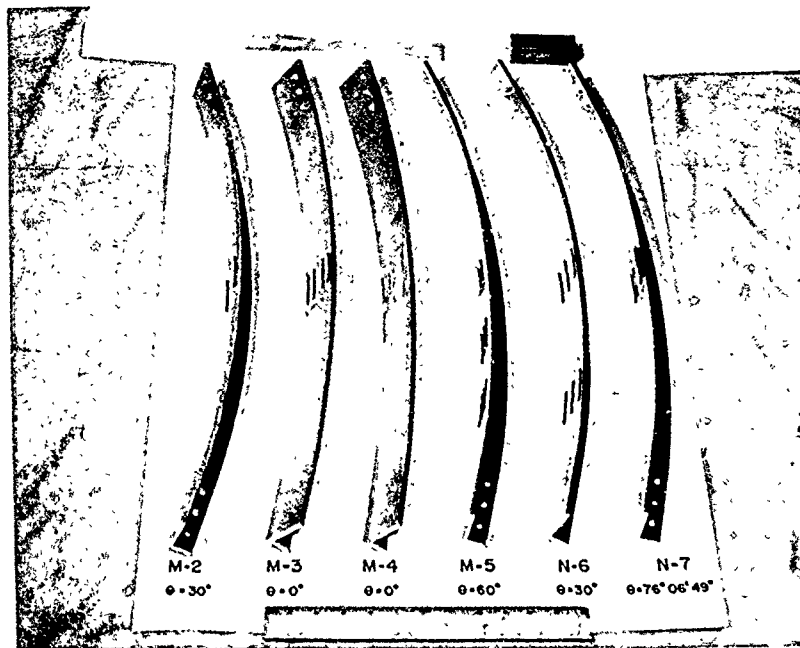
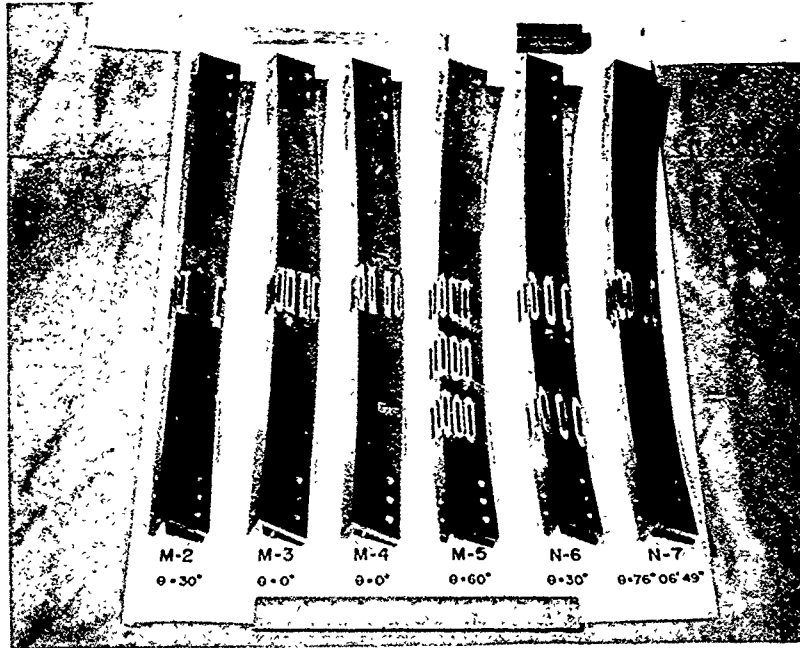


FIG. 2 PHOTOGRAPHS OF BEAMS

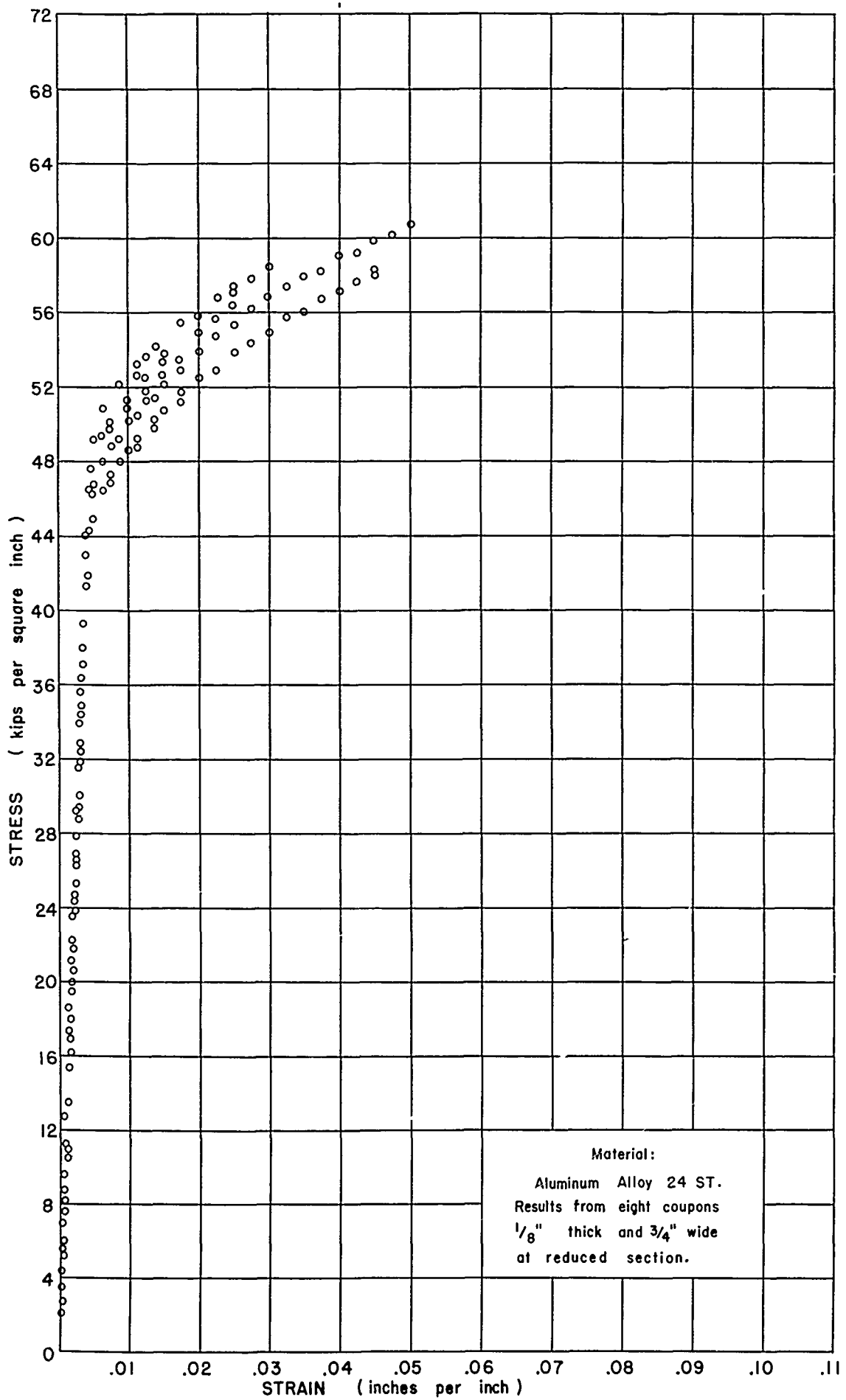


FIG. 3 — TENSION TEST RESULTS

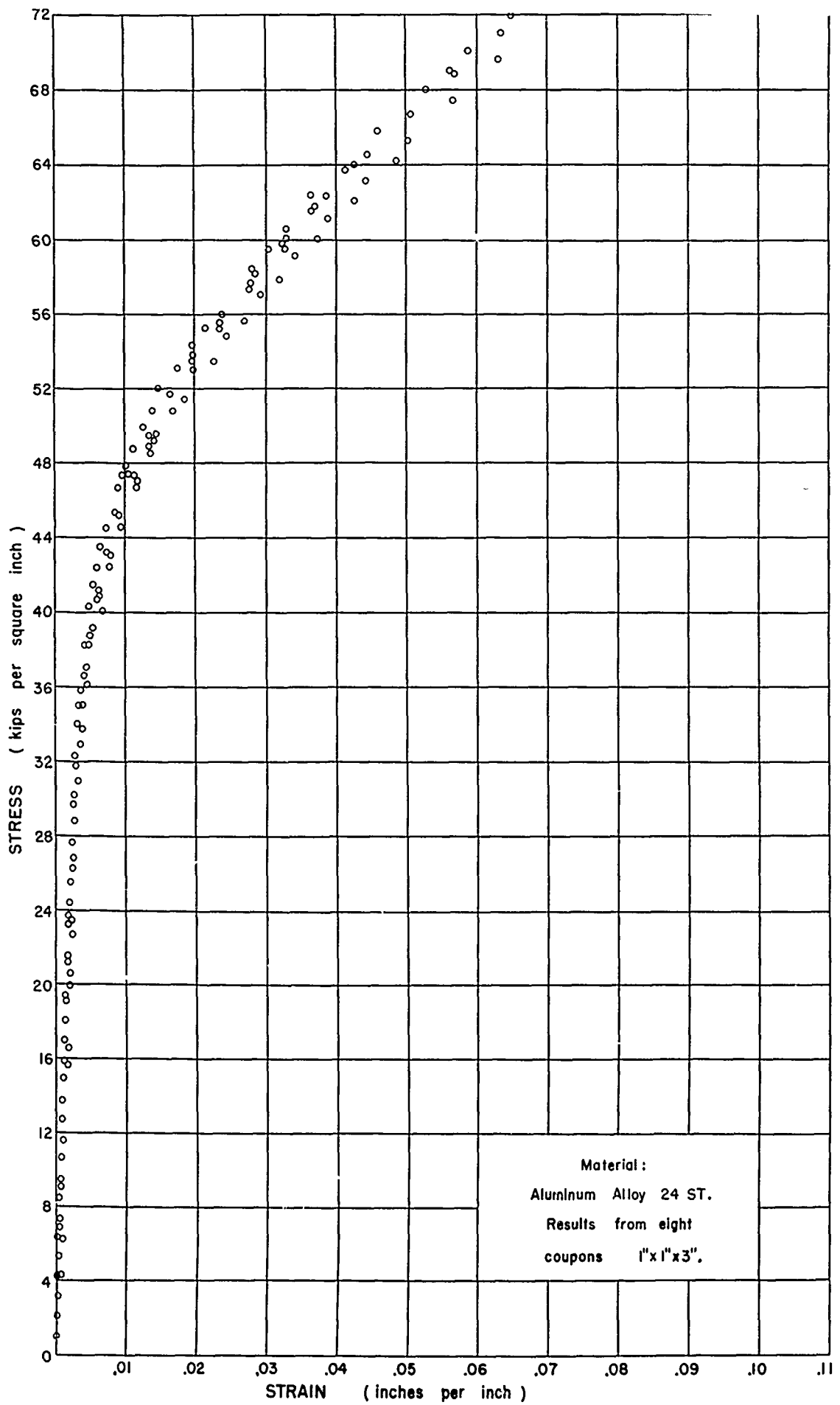


FIG. 4 — COMPRESSION TEST RESULTS

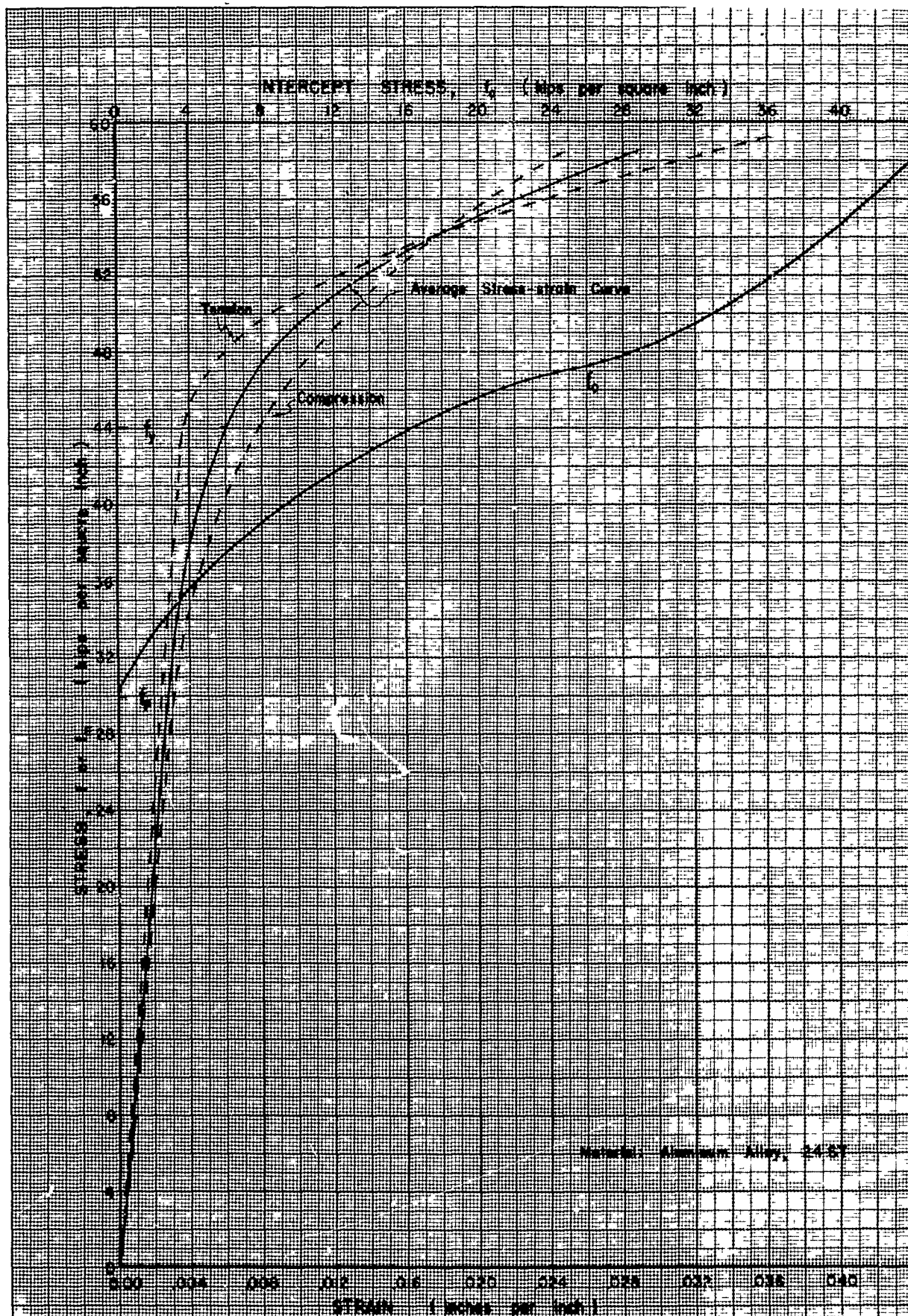
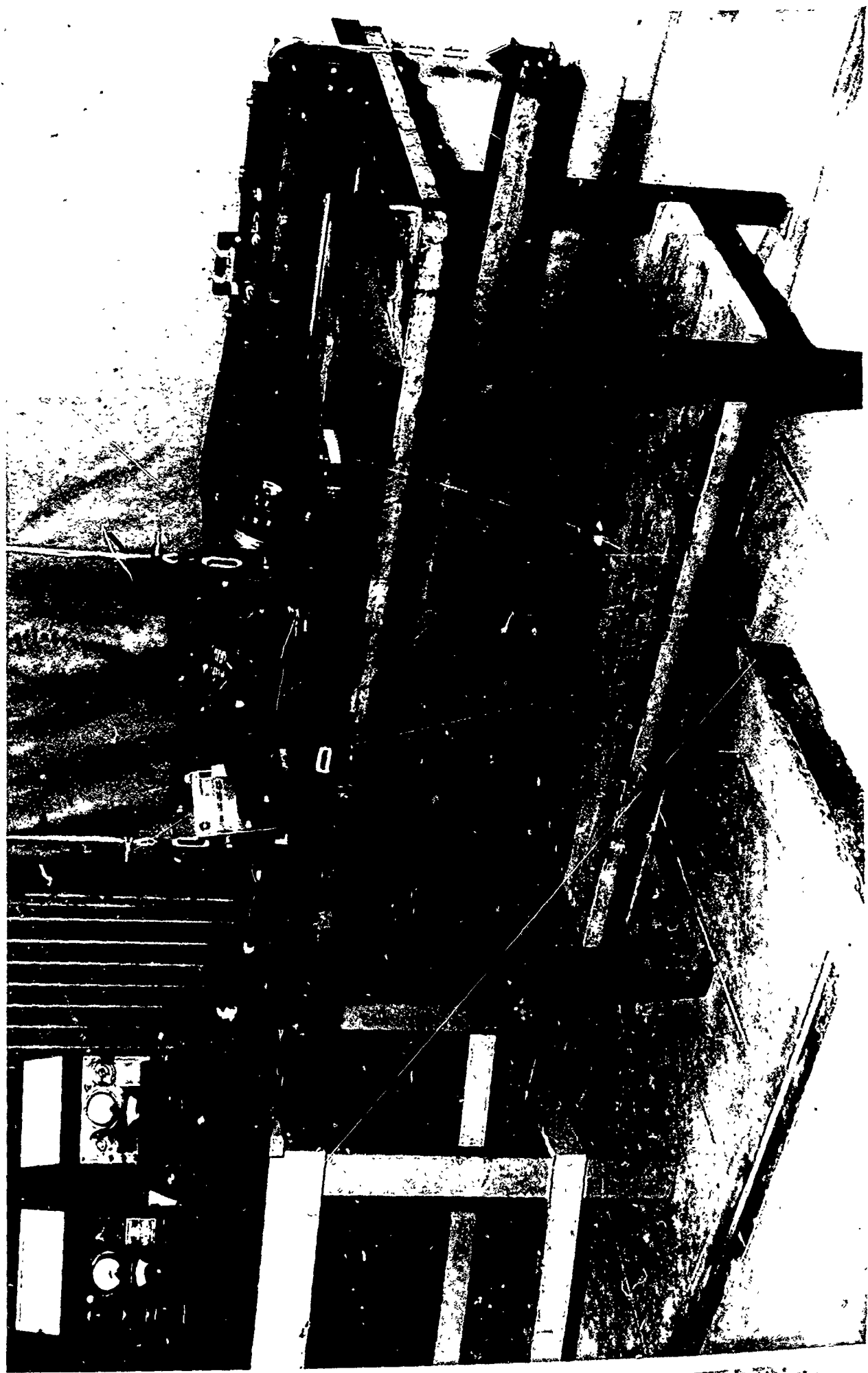


FIG. 5 — RELATIONSHIP BETWEEN STRESS, STRAIN, AND INTERCEPT STRESS, BASED ON AVERAGE STRESS-STRAIN CURVE.

FIGURE 6

FULL VIEW OF PLASTIC BENDING APPARATUS.



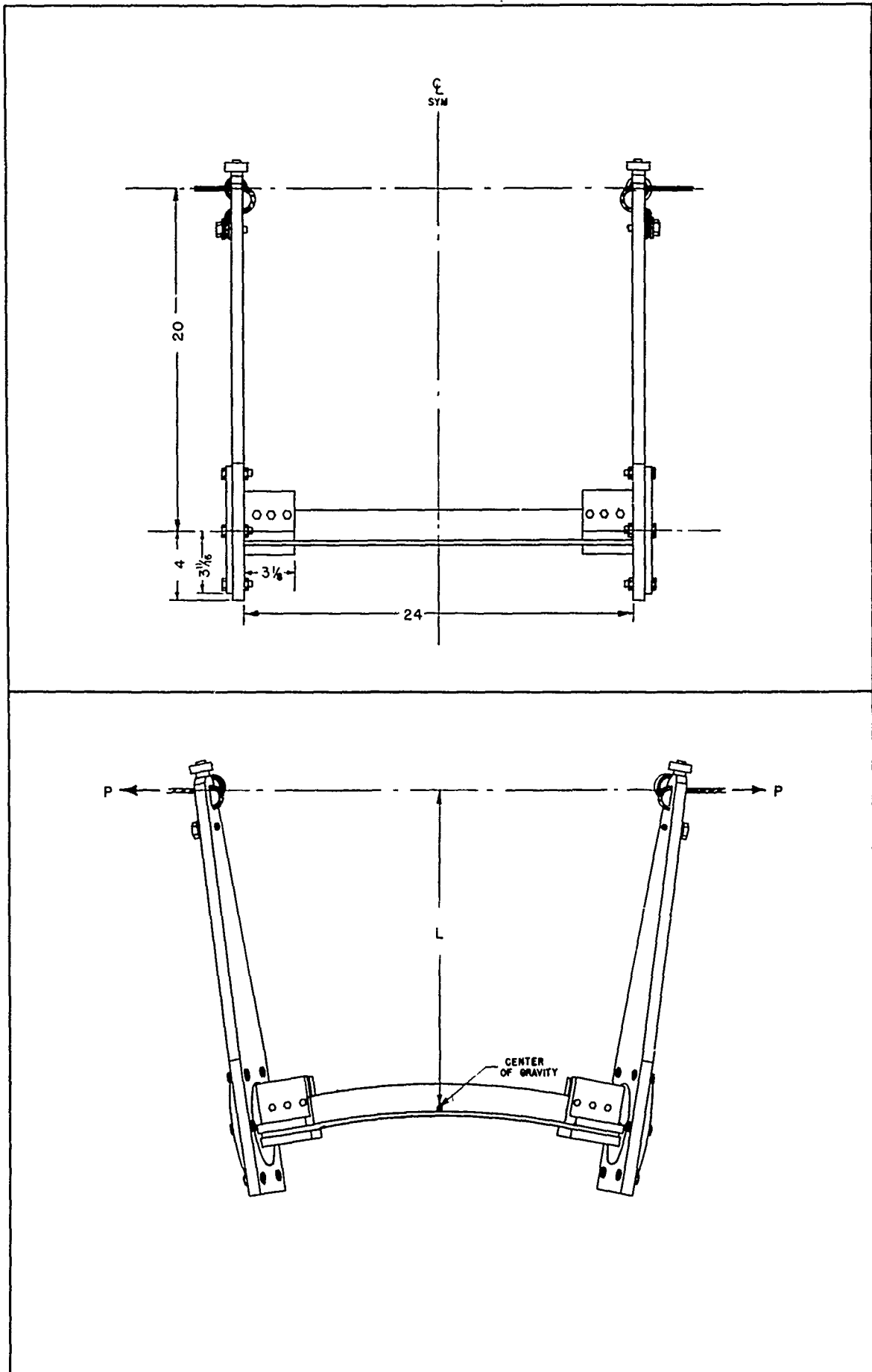
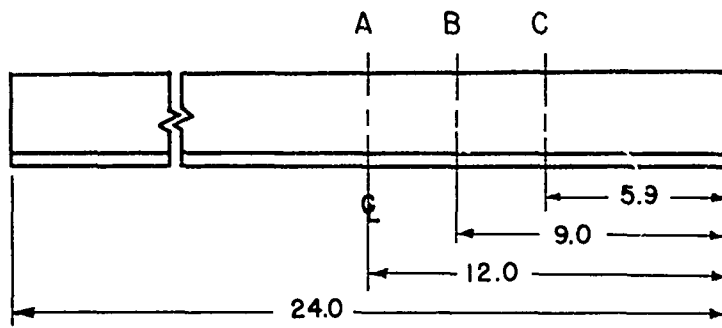
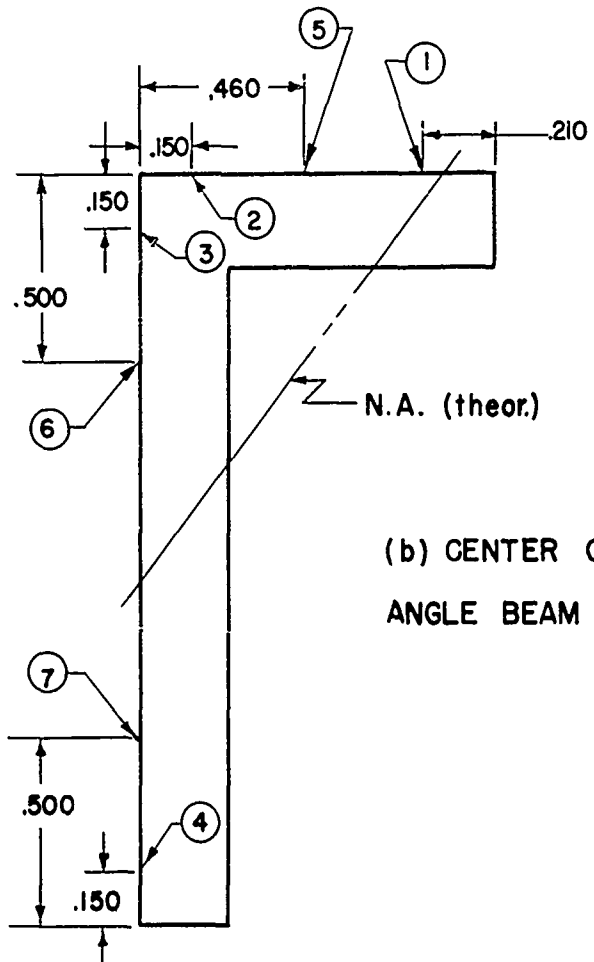


FIG. 7 — PLAN VIEW OF
PLASTIC BENDING APPARATUS

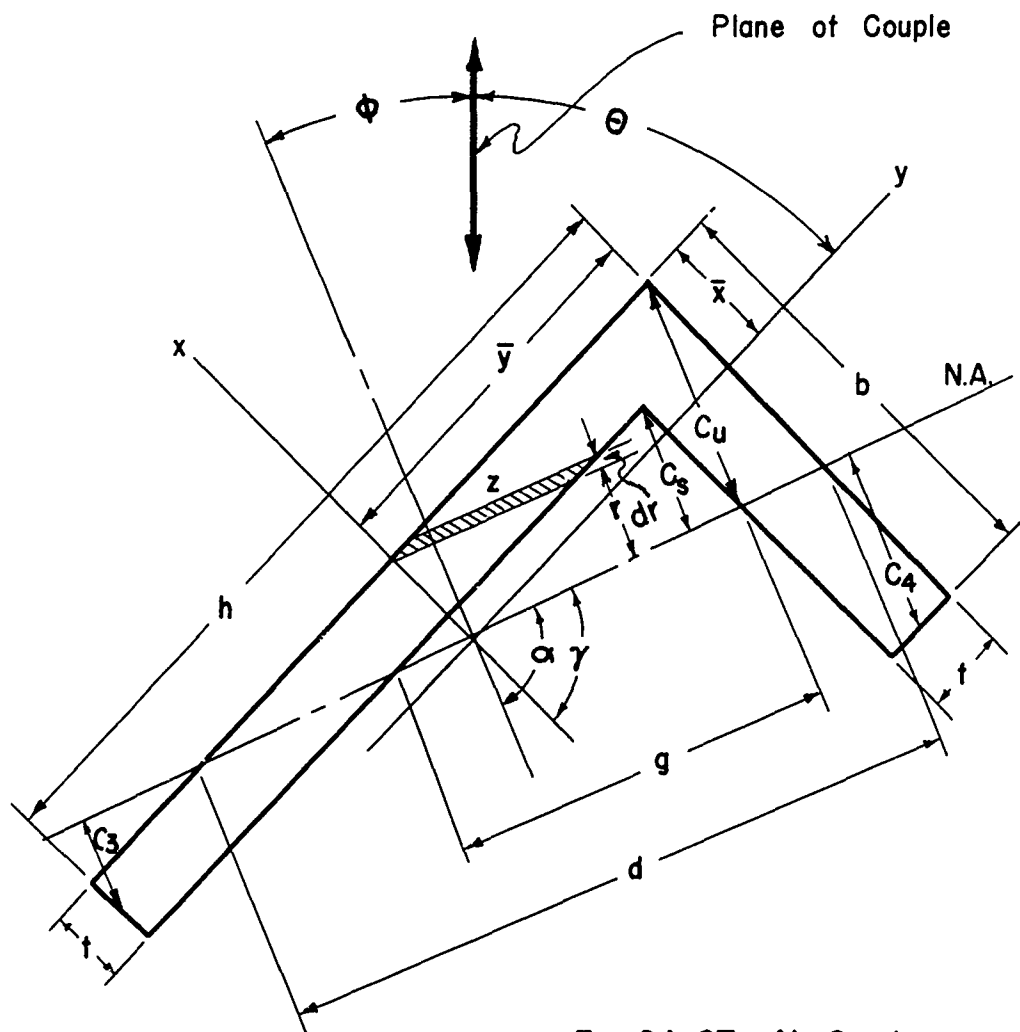


(a) LAYOUT, ANGLE BEAM M-5, $\theta = 60^\circ$



(b) CENTER CROSS SECTION,
ANGLE BEAM M-4, $\theta = 0^\circ$

FIG. 8 — LOCATION OF ELECTRIC STRAIN GAGES



For 24 ST Al. Specimens:

$$\sigma = 91,450 \text{ psi}$$

$$n = 1.1228$$

$$k = 25 \text{ psi}$$

FIG. 9 — CROSS SECTION NOTATION AS USED IN THE
EXPONENTIAL SOLUTION FOR M_{th}

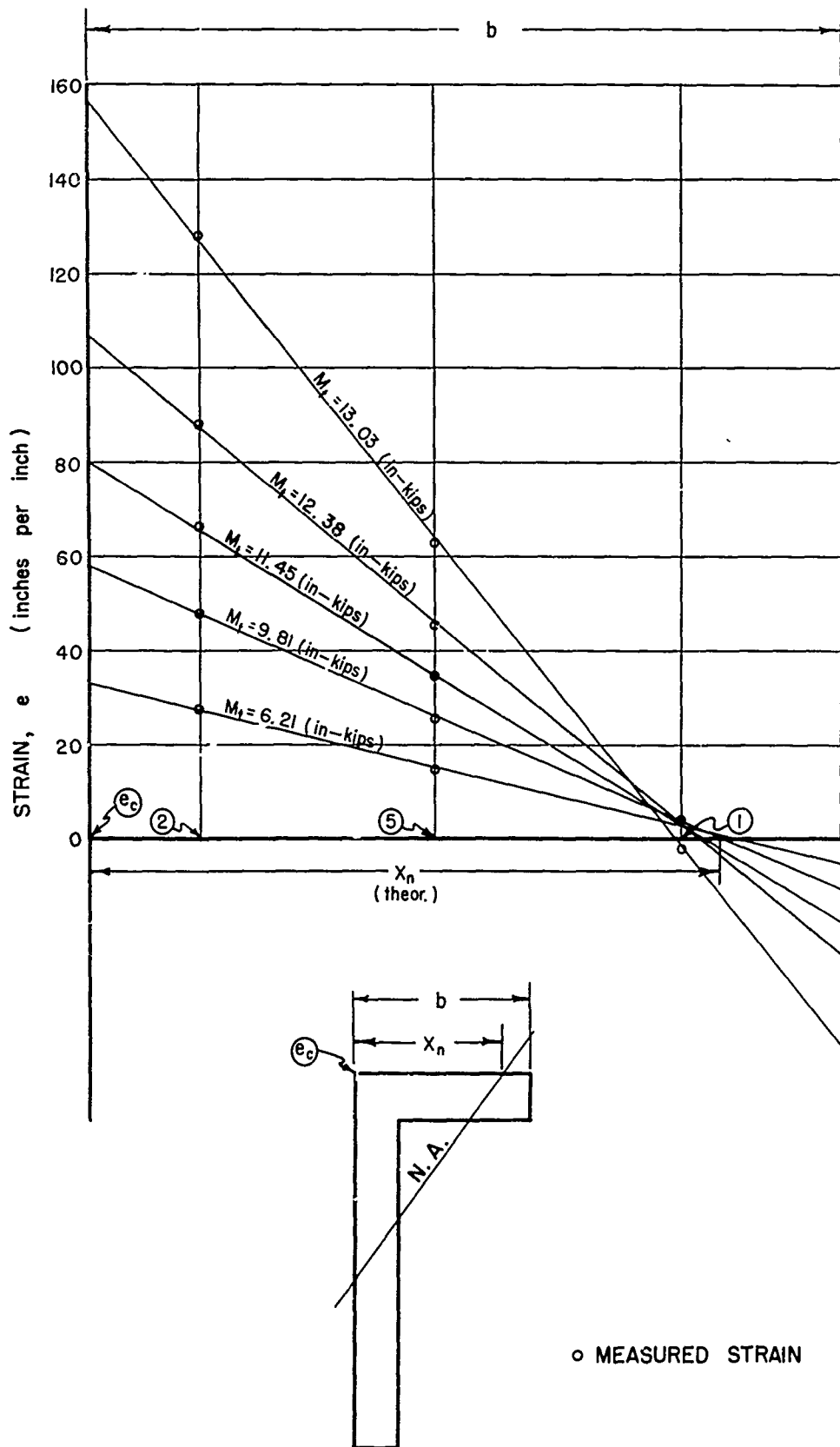


FIG. 10 — SAMPLE GRAPHICAL SOLUTION FOR OBTAINING X_n AND e_c ; ANGLE BEAM M-4, $\theta = 0^\circ$.

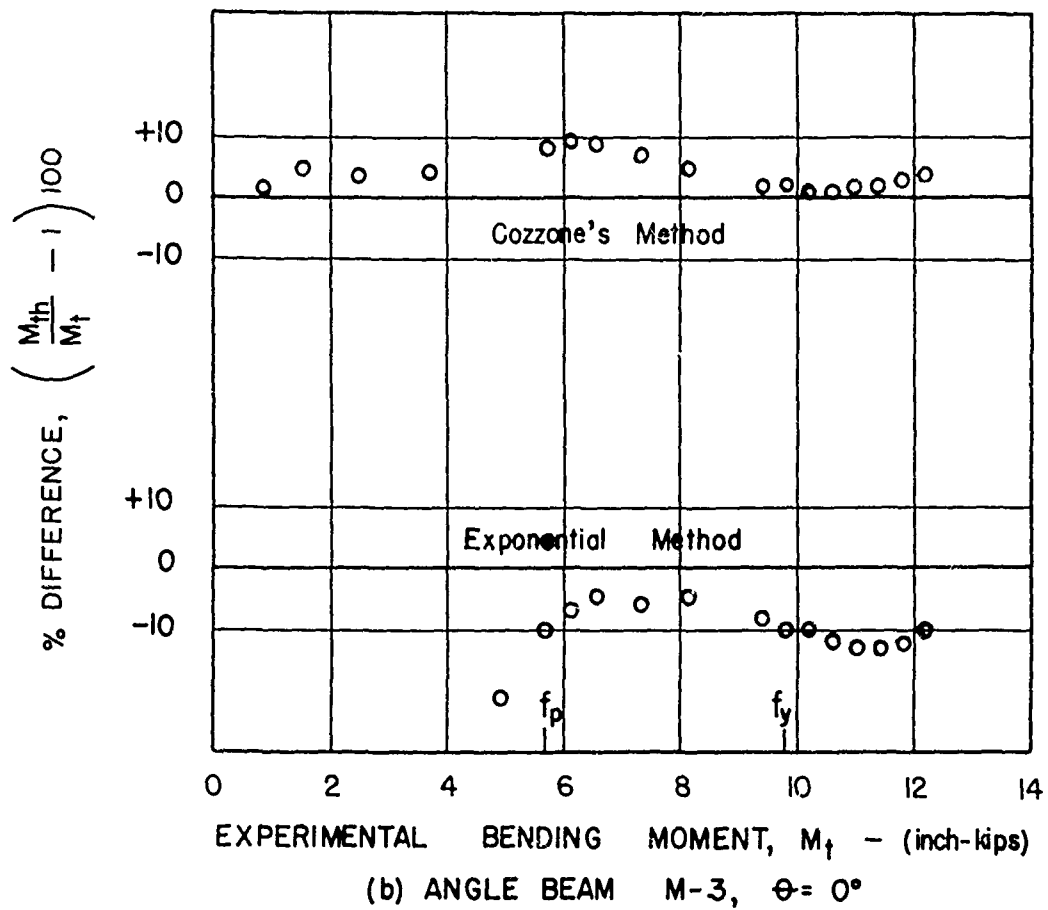
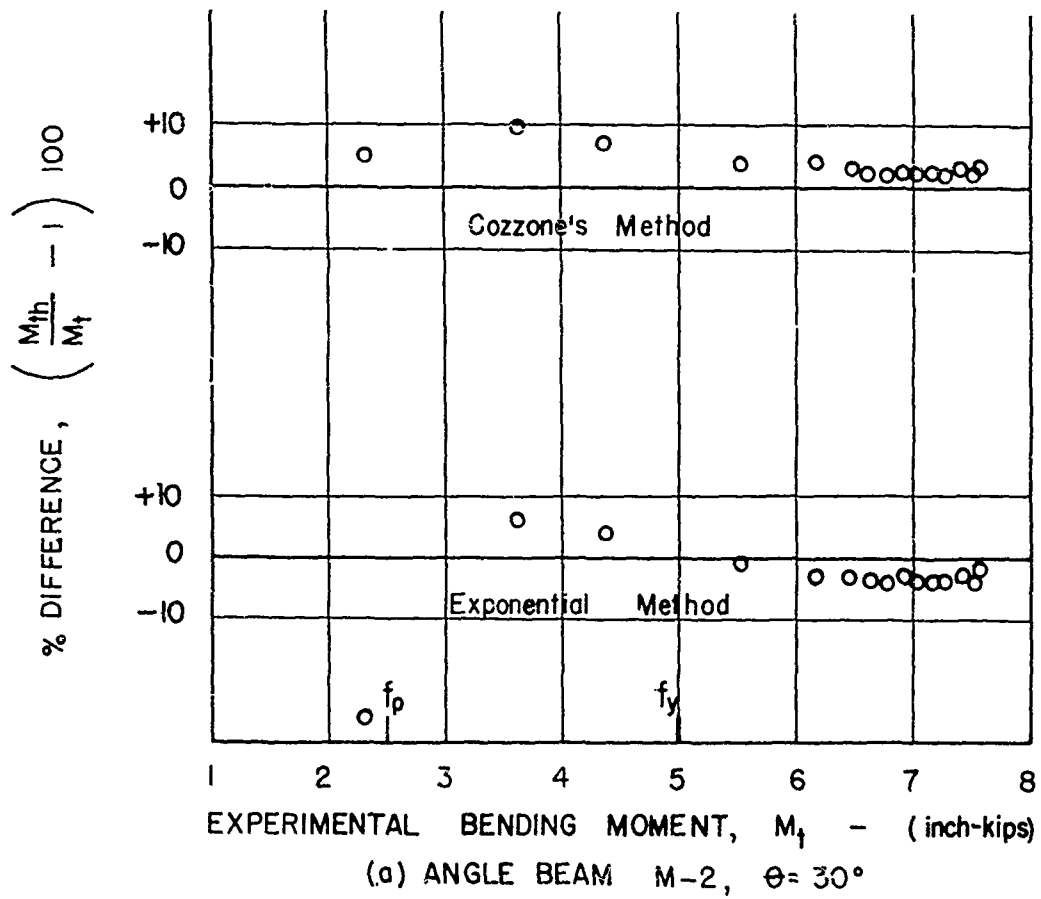


FIG. II -% DIFFERENCE BETWEEN EXPERIMENTAL AND COMPUTED BENDING MOMENTS FOR ANGLE BEAMS M-2 & M-3

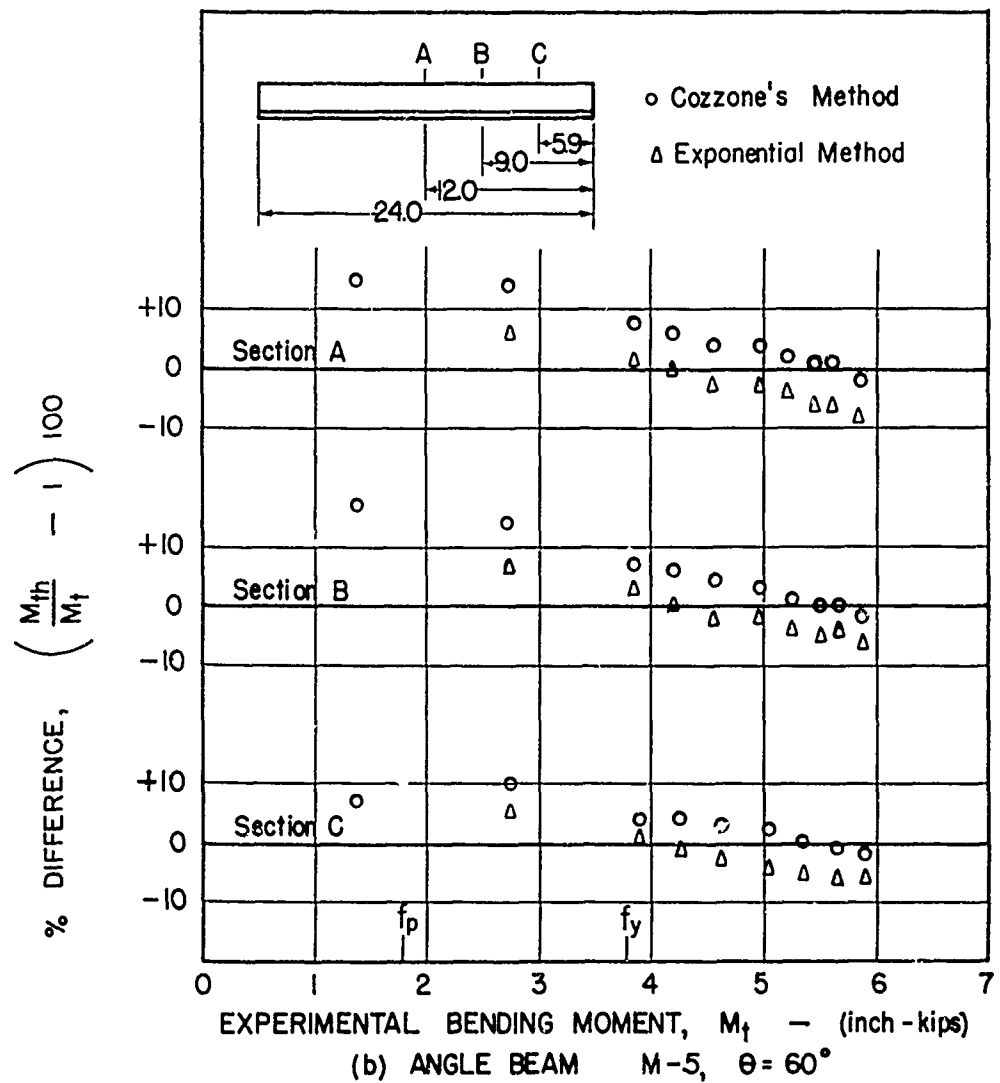
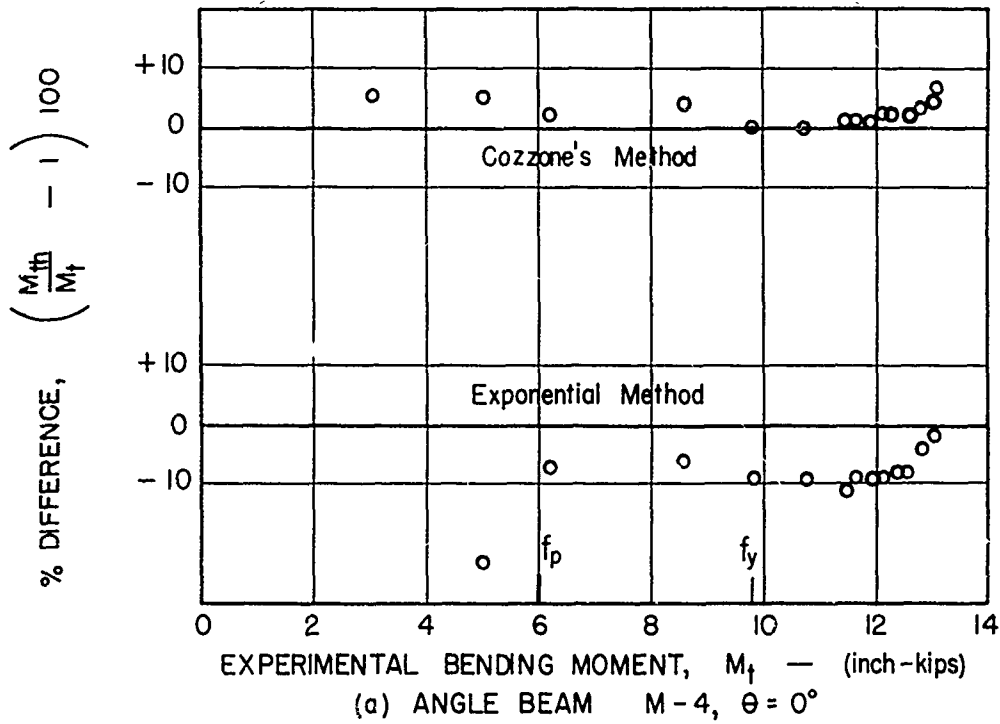


FIG. 12 - % DIFFERENCE BETWEEN EXPERIMENTAL AND COMPUTED BENDING MOMENTS FOR ANGLE BEAMS M-4 & M-5

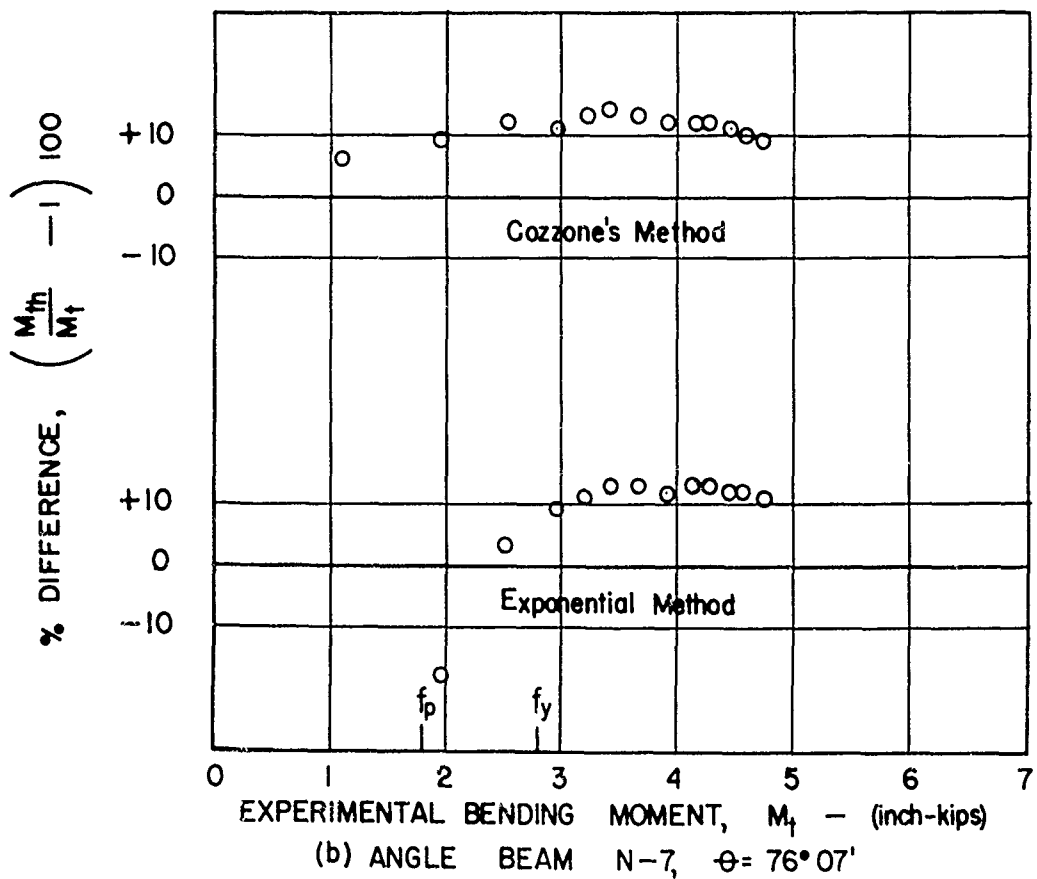
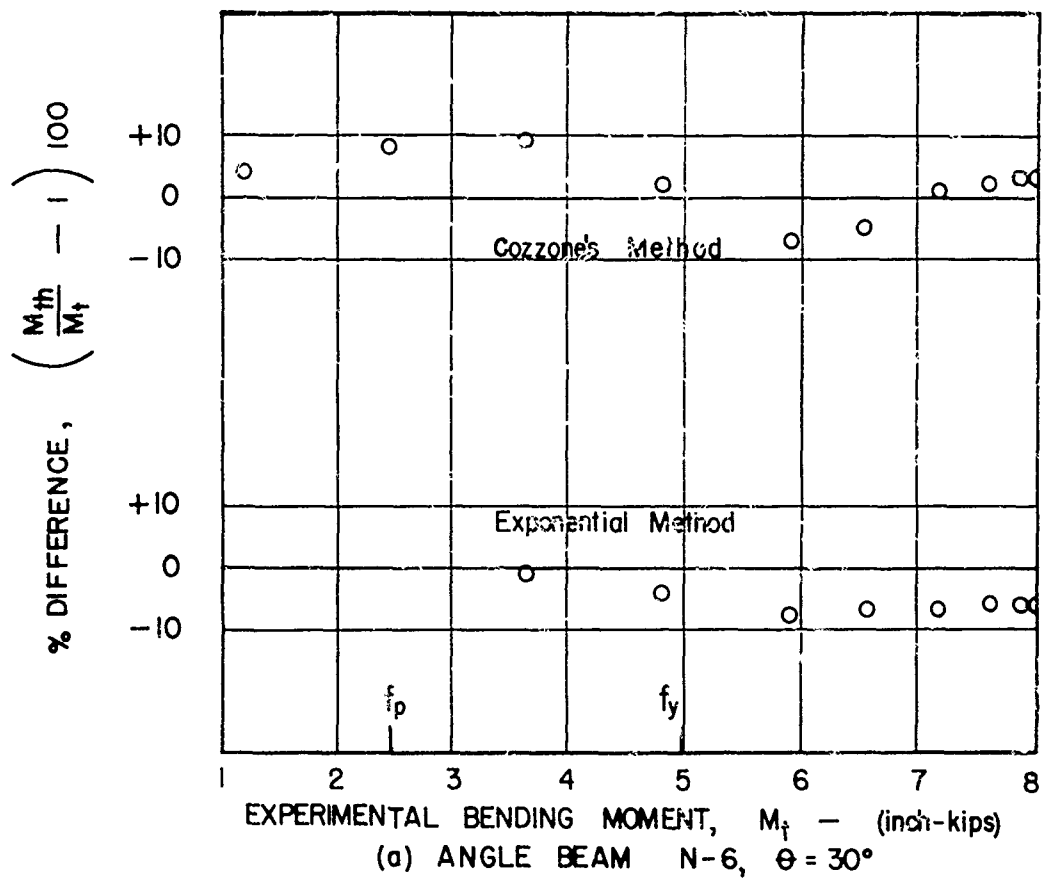
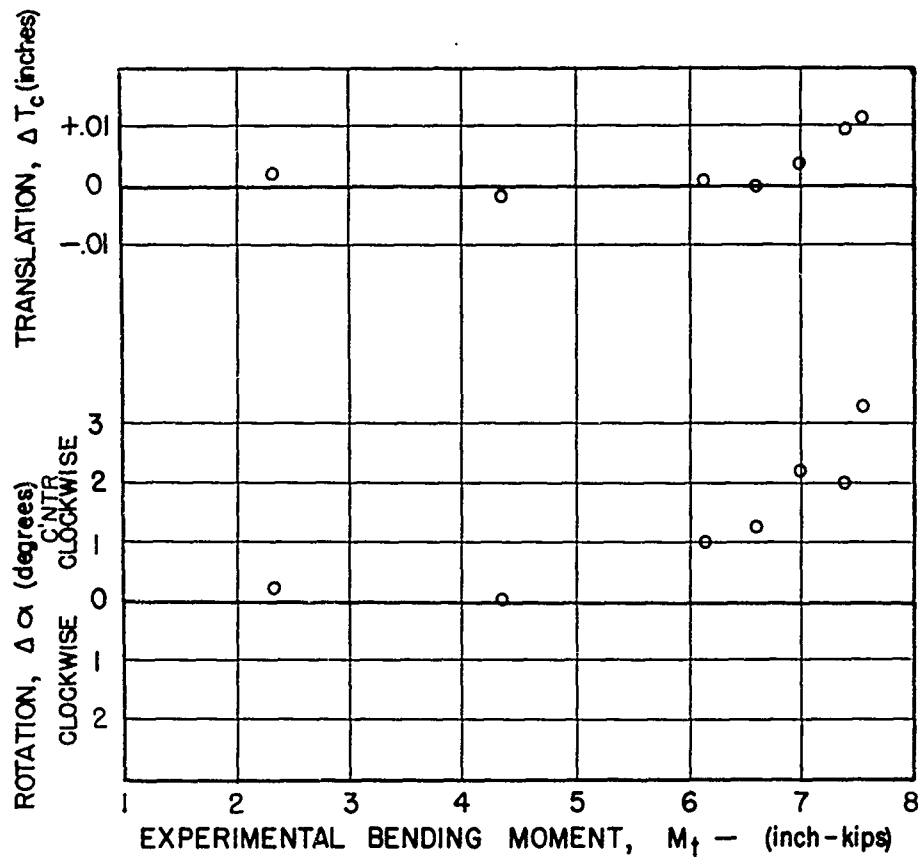
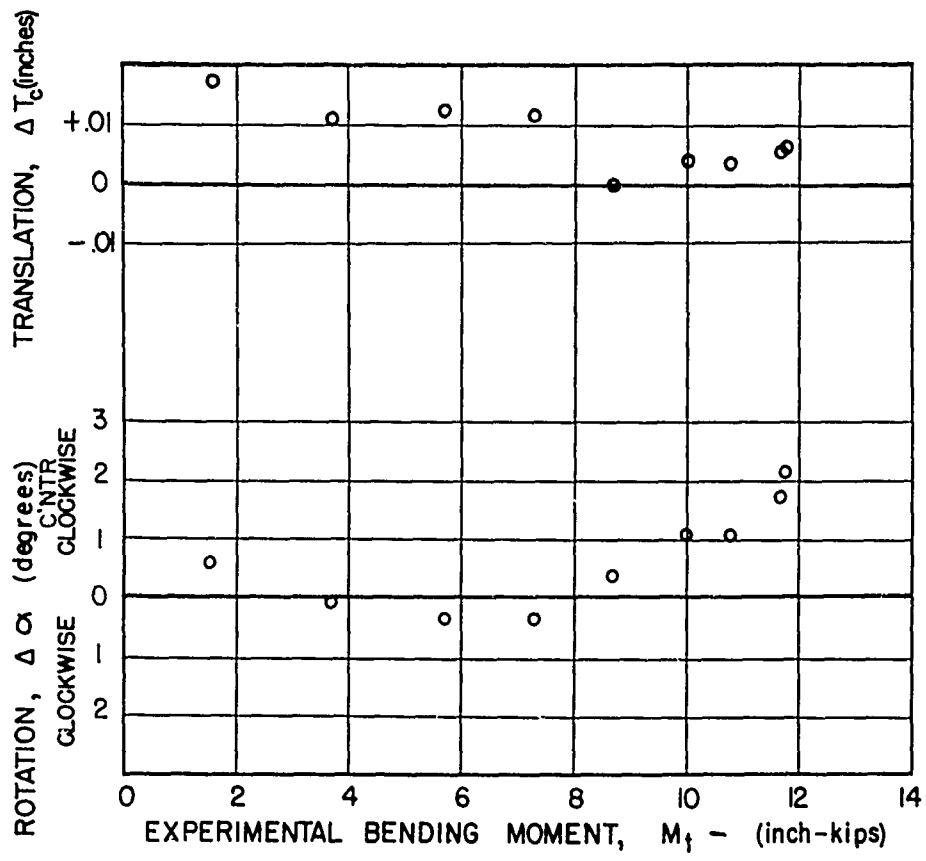


FIG. 13 -% DIFFERENCE BETWEEN EXPERIMENTAL AND COMPUTED BENDING MOMENTS FOR ANGLE BEAMS N-6 & N-7

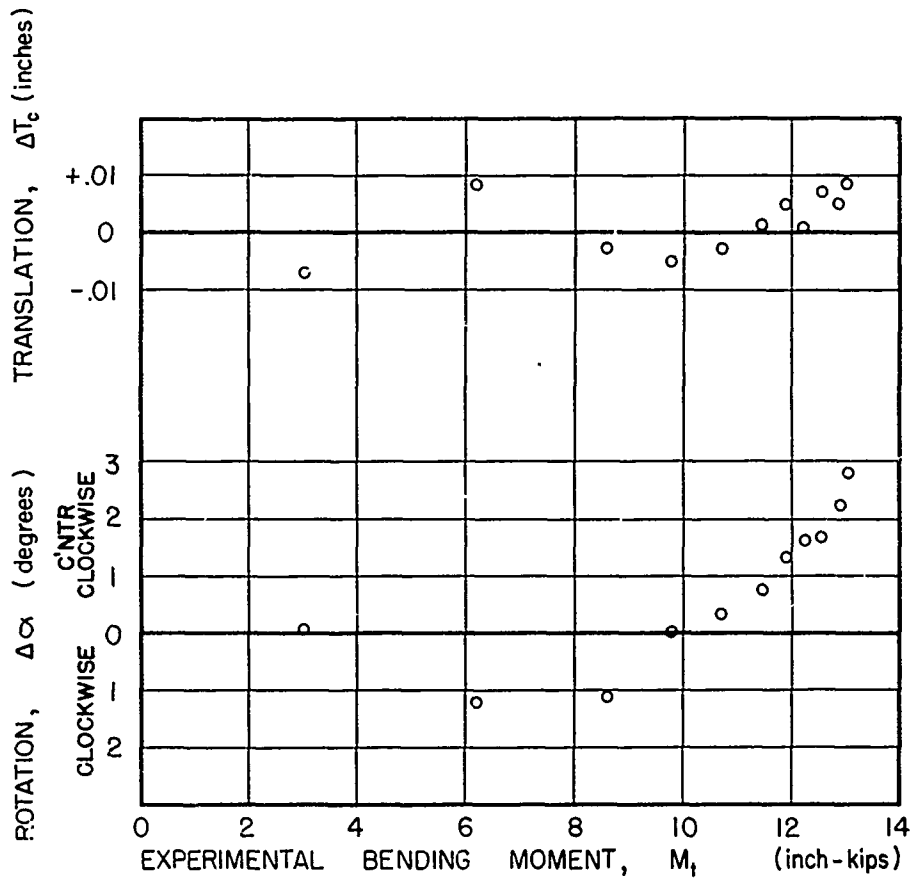


(a) ANGLE BEAM M-2, $\theta = 30^\circ$

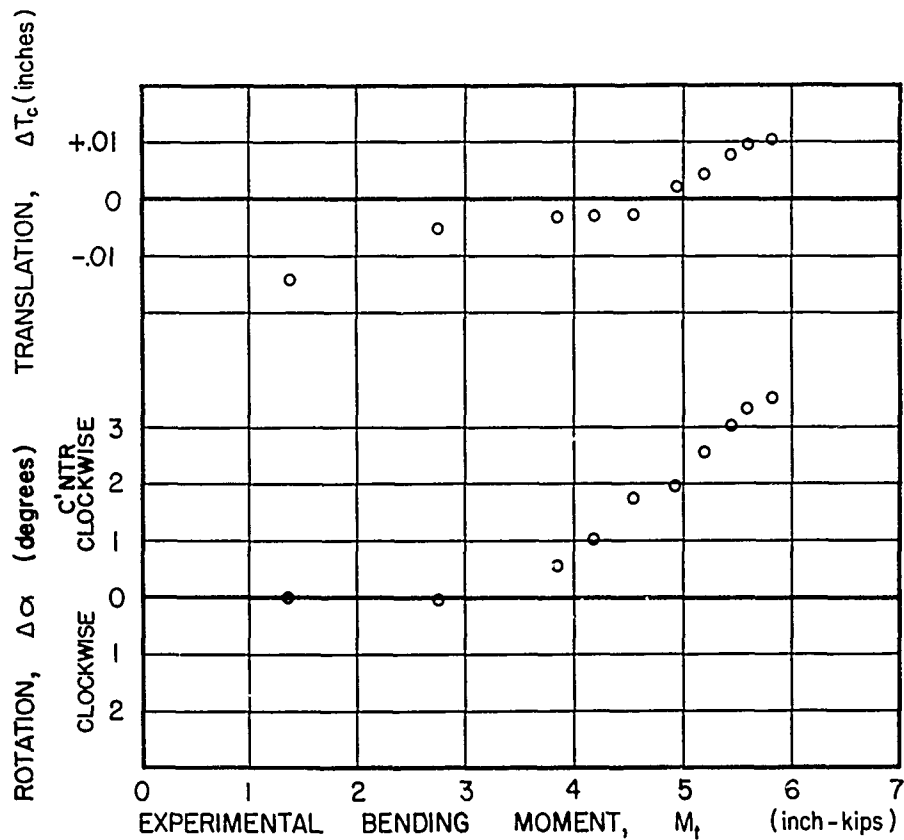


(b) ANGLE BEAM M-3, $\theta = 0^\circ$

FIG. 14 - CHANGE IN THE POSITION OF THE NEUTRAL AXIS FOR ANGLE BEAMS M-2 & M-3

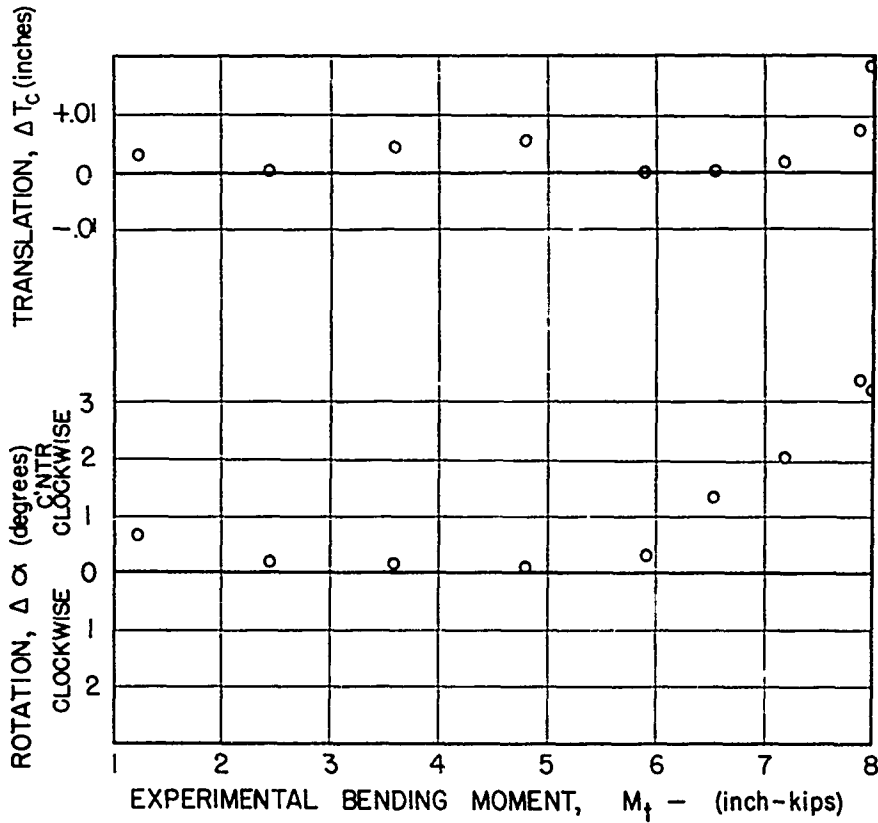


(a) ANGLE BEAM M-4, $\theta = 0^\circ$

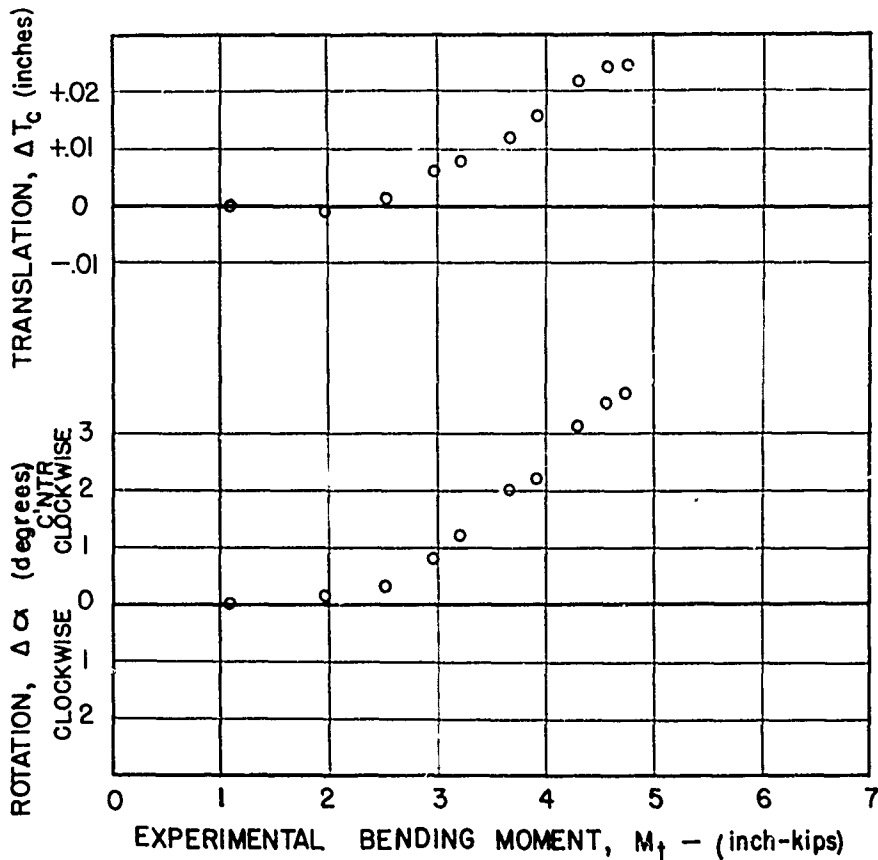


(b) ANGLE BEAM M-5, $\theta = 60^\circ$

FIG. 15 — CHANGE IN THE POSITION OF THE NEUTRAL AXIS FOR ANGLE BEAMS M-4 & M-5

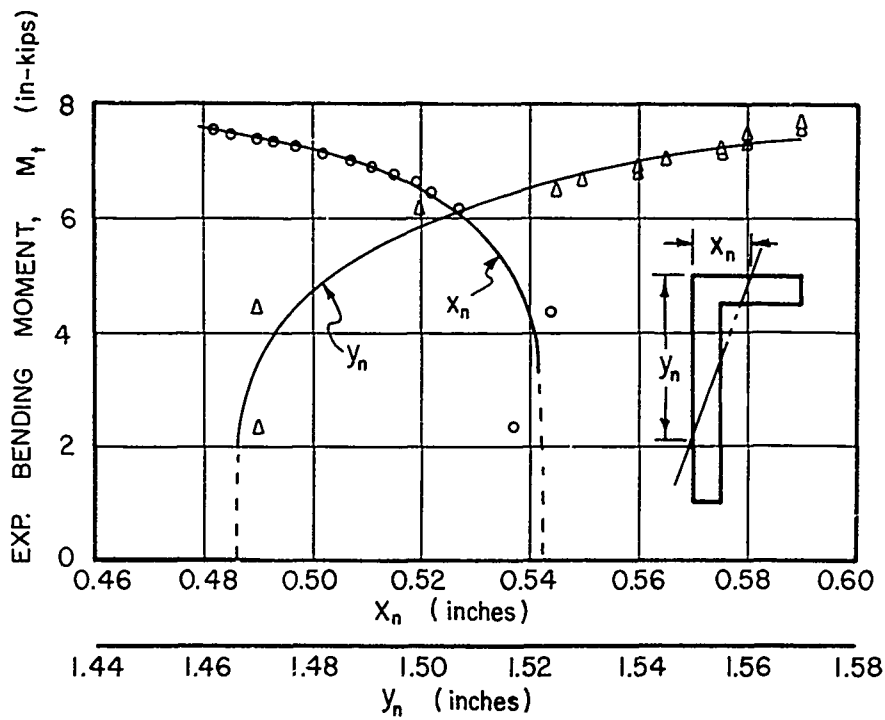


(a) ANGLE BEAM N-6, $\theta = 30^\circ$

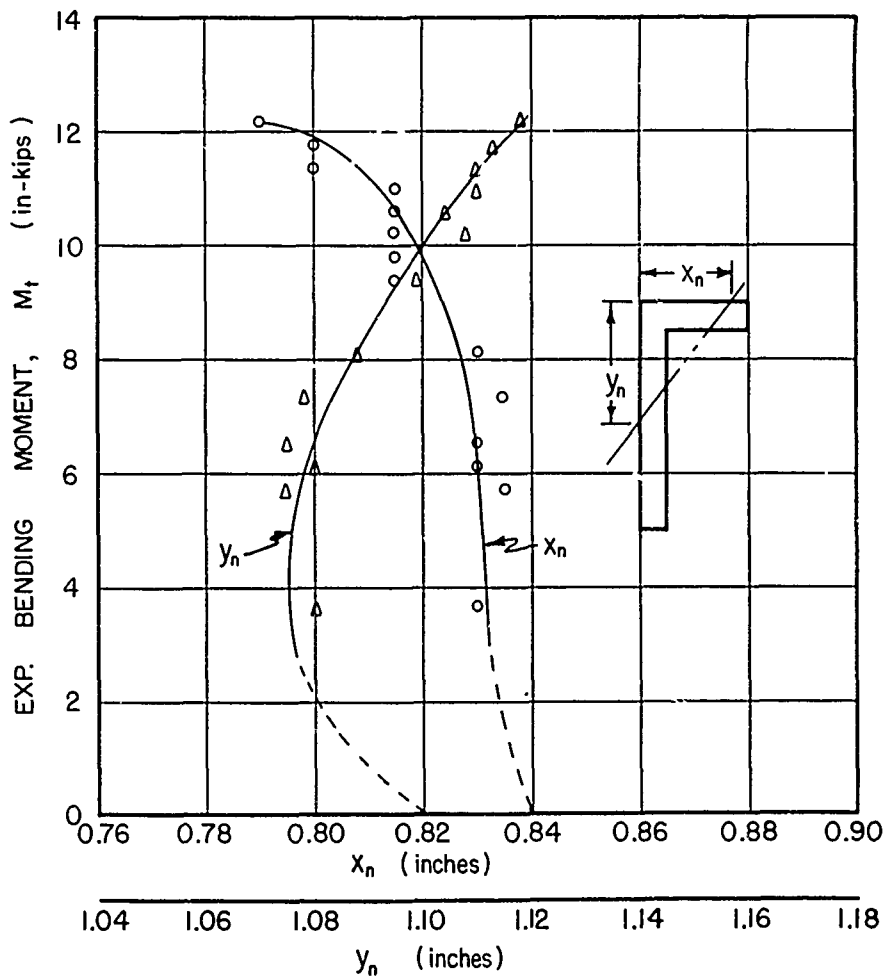


(b) ANGLE BEAM N-7, $\theta = 76^\circ 07'$

FIG. 16 - CHANGE IN THE POSITION OF THE NEUTRAL AXIS FOR ANGLE BEAMS N-6 & N-7

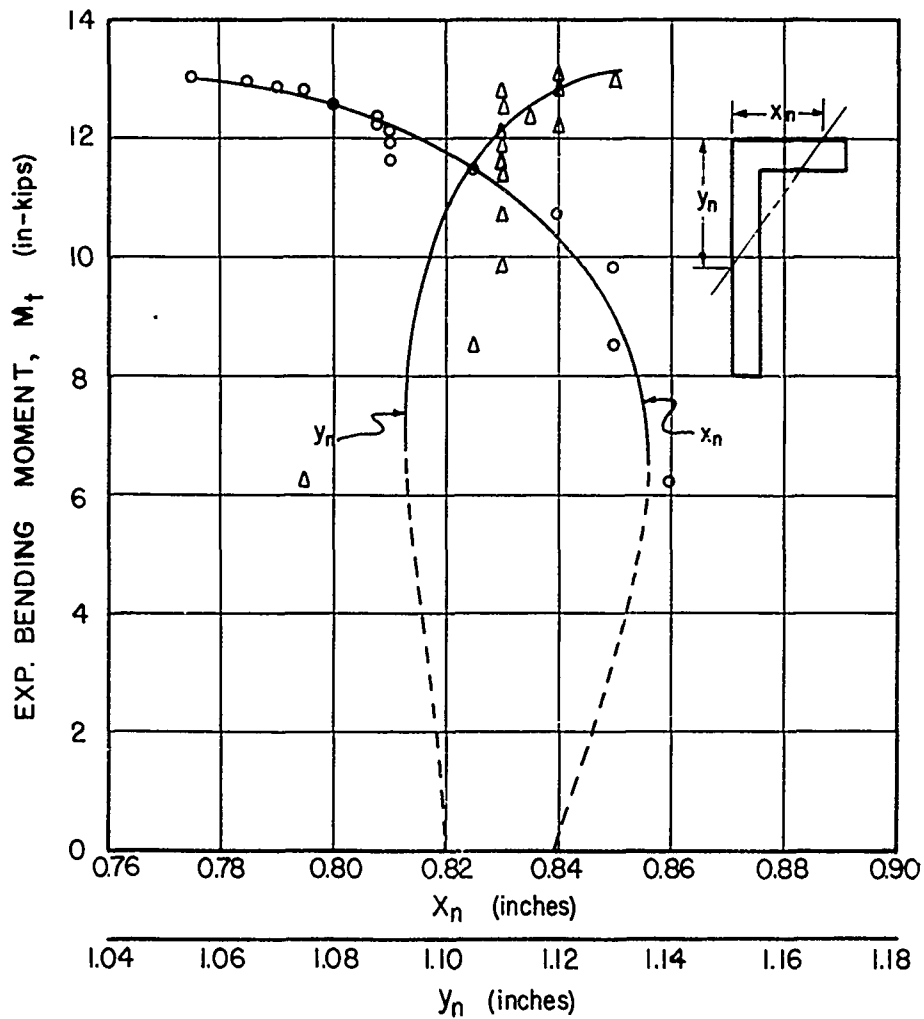


(a) ANGLE BEAM M-2, $\theta = 30^\circ$

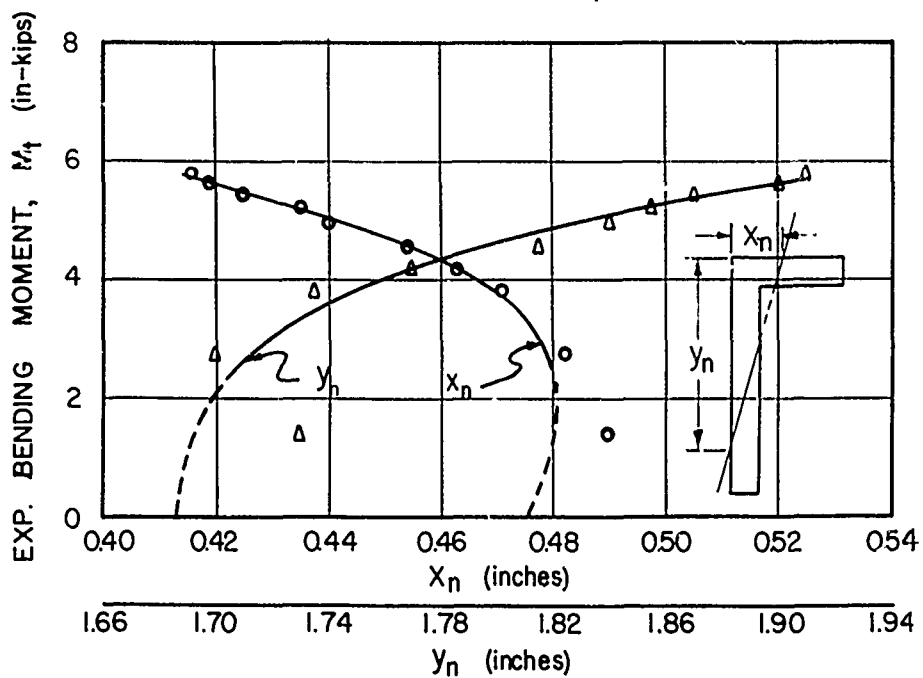


(b) ANGLE BEAM M-3, $\theta = 0^\circ$

FIG. 17 — NEUTRAL AXIS LOCATION FOR ANGLE BEAMS M-2 AND M-3.

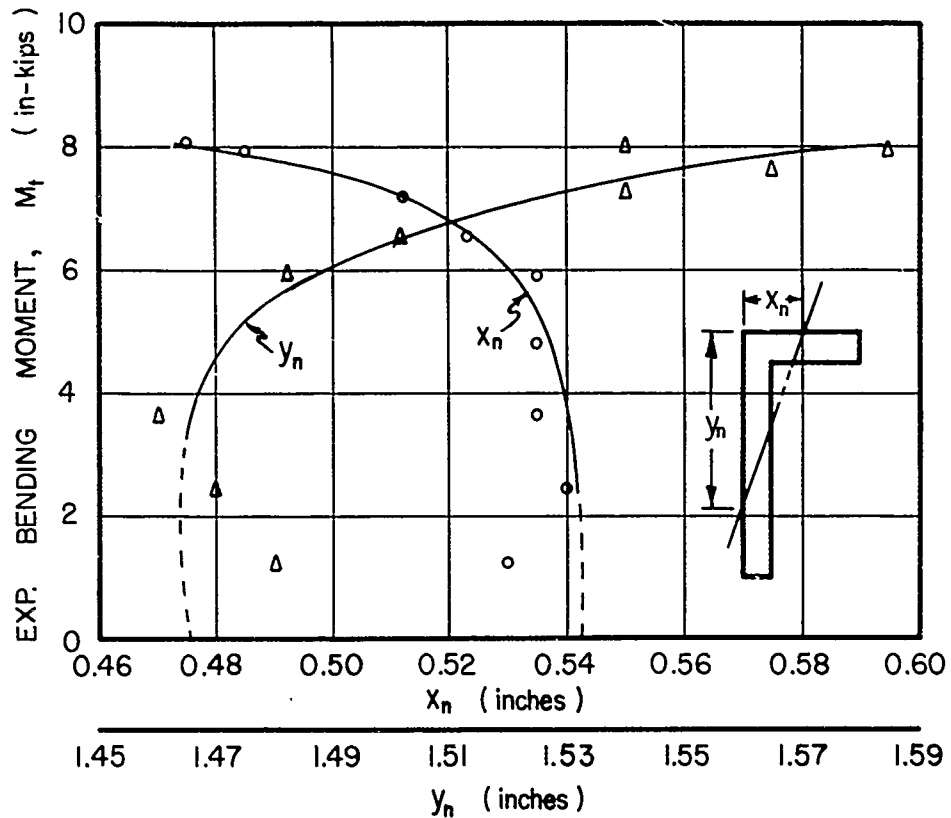


(a) ANGLE BEAM M-4, $\theta = 0^\circ$

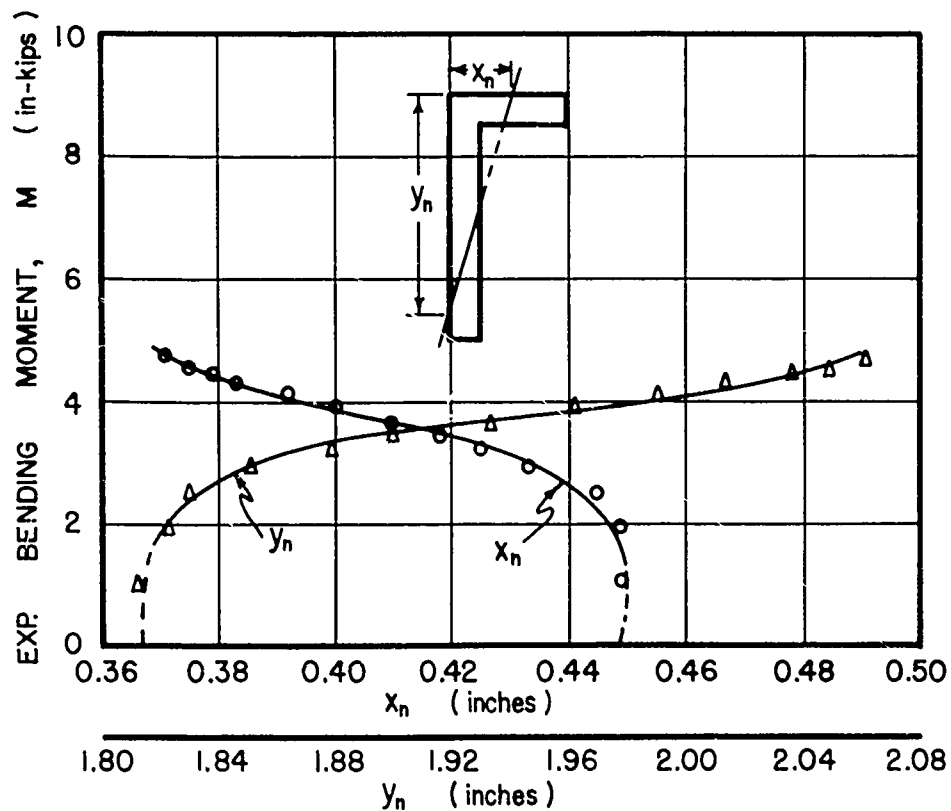


(b) ANGLE BEAM M-5, $\theta = 60^\circ$

FIG. 18 — NEUTRAL AXIS LOCATION FOR ANGLE BEAMS M-4 AND M-5



(a) ANGLE BEAM N-6, $\theta = 30^\circ$



(b) ANGLE BEAM N-7, $\theta = 76^\circ 07'$

FIG. 19 — NEUTRAL AXIS LOCATION FOR ANGLE BEAMS N-6 AND N-7

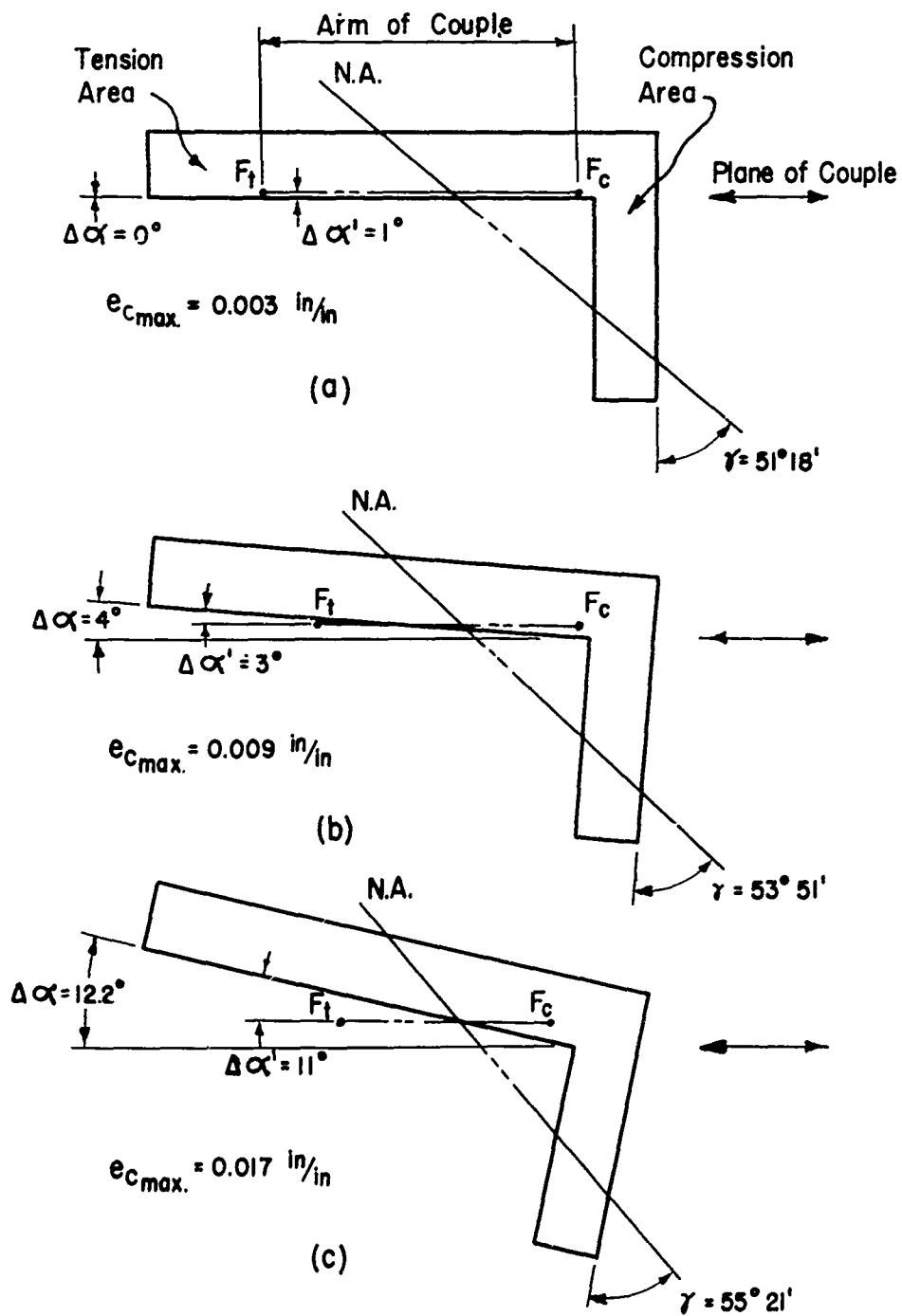


FIG. 20 — LOCATION OF RESISTING COUPLE AT MID-SPAN
FOR THREE STAGES OF ROTATION

ANGLE BEAM M-4, $\theta = 0^\circ$

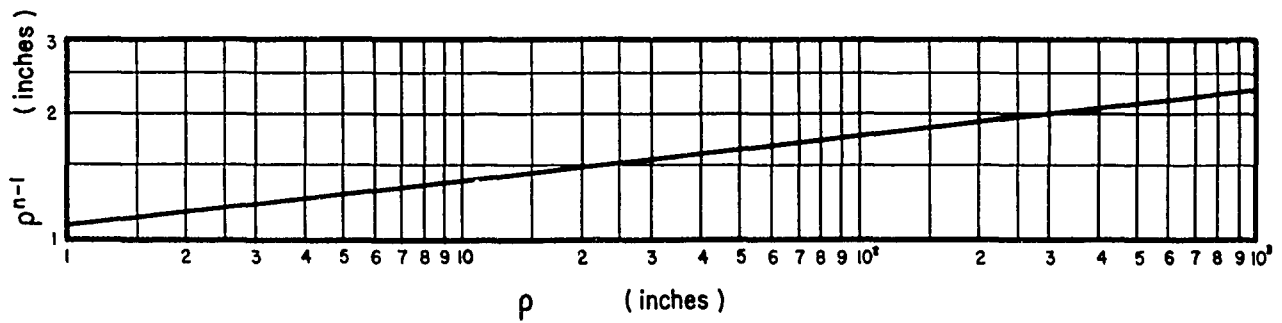
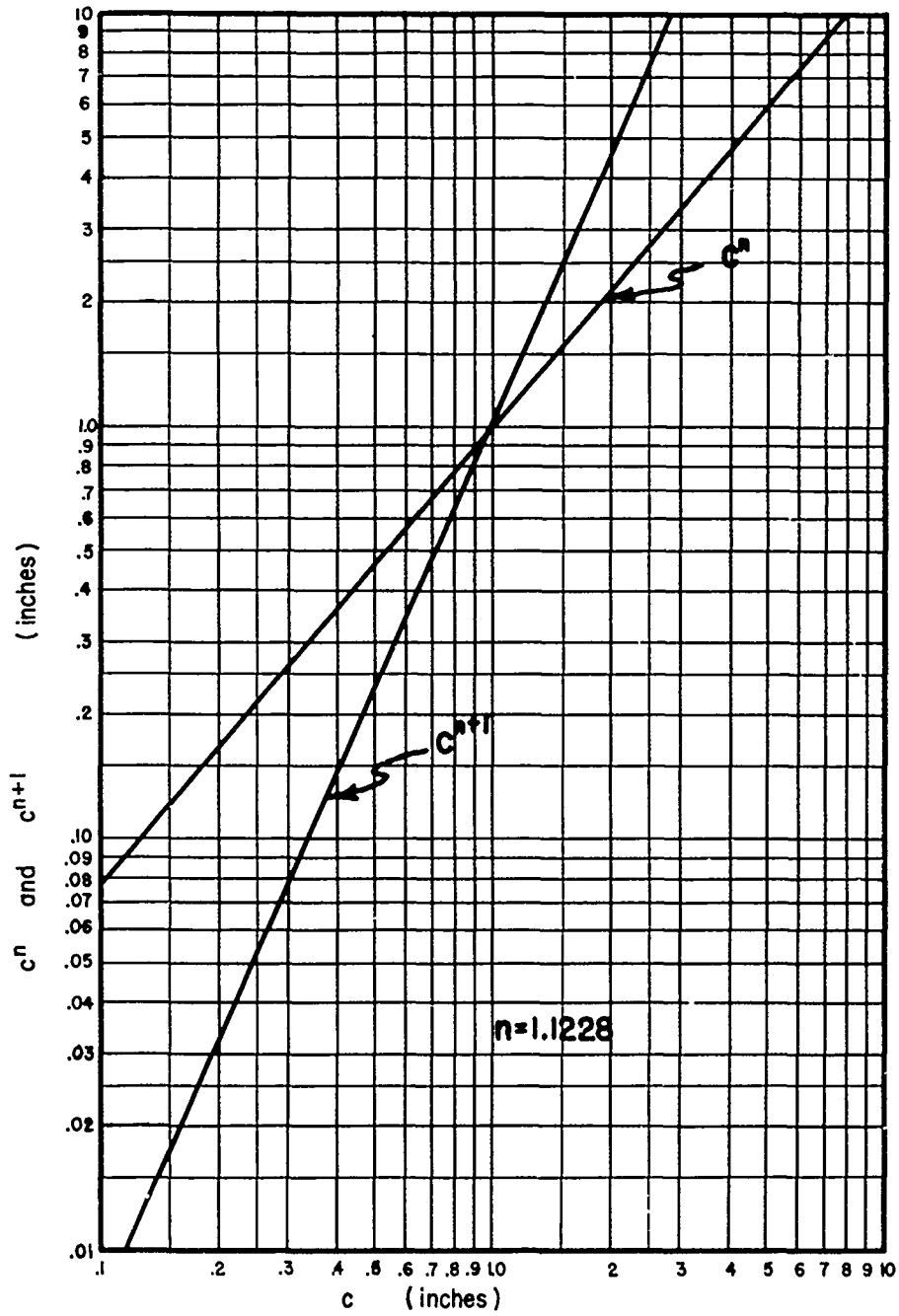


FIG. 21 — VALUES OF ρ AND c FOR USE IN THE EXPONENTIAL EQUATION

Table No. 1 - TEST RESULTS
Angle Beam M-2
 $\theta = 30^\circ$

Total load (kips)	Mem. arm (in)	Expt. bend. mom. (in-kips)	Rotation (deg.)	Neutral axis location (in)	x_n (in)	y_n (in)	e_c (in/in $\times 10^{-4}$)	ϵ_t	Theoret. bending moment (Cos.) (in-kips)	Diff. (Cos.) (%)	Theoret. bending moment (Expon.) (in-kips)	Diff. (Expon.) (%)
P	L	M_t	θ	x_n	y_n	e_c	ϵ_t	M_{th}			M_{th}	
0	20.00	0	0	0.543	1.466	0	0	0	0	-	0	-
0.12	19.80	2.34	0.4	0.537	1.470	26.0	26.9	2.45	5	1.93	1.93	0
0.225	19.48	4.36	1.0	0.544	1.470	50.0	50.5	4.67	7	4.55	4.55	4
0.325	18.87	6.15	2.5	0.527	1.500	87.8	94.0	6.38	4	5.98	5.98	-3
0.34	18.65	6.46	3.0	0.522	1.525	99.0	108	6.66	3	6.25	6.25	-3
0.36	18.53	6.62	3.4	0.519	1.530	106	117	6.78	2	6.39	6.39	-4
0.37	18.40	6.76	3.8	0.515	1.540	113	126	6.89	2	6.48	6.48	-4
0.38	18.25	6.89	4.2	0.511	1.540	121	137	7.05	2	6.66	6.66	-3
0.39	18.10	7.02	4.7	0.507	1.545	128	147	7.16	2	6.76	6.76	-4
0.395	17.95	7.02	5.2	0.502	1.550	137	160	7.27	2	6.86	6.86	-4
0.42	17.75	7.24	6.0	0.497	1.550	146	174	7.38	2	6.97	6.97	-4
0.42	17.57	7.24	6.7	0.493	1.560	155	187	7.49	2	7.05	7.05	-4
0.425	17.36	7.39	-	0.490	1.560	164	202	7.60	3	7.15	7.15	-3
0.44	17.10	7.50	8.0	0.485	1.570	174	218	7.70	2	7.24	7.24	-4
0.45	16.85	7.55	8.5	0.482	1.570	184	232	7.77	3	7.39	7.39	-2

^aFrom graphical solution assuming linear variation of strain.

^bResisting moment of compression and tension areas computed separately by Coszone's method assuming neutral axis stationary:

$$M'_{th} = \frac{I_c}{c_c} \frac{1}{\cos \phi} \left[f_{mc} f_{oc} (k_c - 1) \right] = 0.0427 (f_{mc} + 0.930 f_{oc})$$

$$M''_{th} = \frac{I_t}{c_t} \frac{1}{\cos \phi} \left[f_{mt} + f_{ot} (k_t - 1) \right] = 0.0434 (f_{mt} + 0.863 f_{ot})$$

$$M_{th} = M'_{th} + M''_{th}$$

^cExponential equation: $M_{th} = \frac{12000}{\rho} \frac{1}{n-1} - 22.33 \rho$

^dTheoretical value.

^eCounterclockwise, referred to Figure 1.

Table No. 2 - TEST RESULTS
Angle Beam M-3
 $\theta = 0^\circ$

Total load (kips)	Mem. arm (in)	Expt. bend. mea.	Rotation (deg.)	Neutral axis location (in)	x_n (in)	y_n (in)	Outer fiber strain	ϵ_c	ω_t	Theoret. bending moment (Cosz.)	Diff. (Cosz.) (%)	Theoret. bending moment (Expon.)	Diff. (Expon.) (%)
P	L	M_t			x_n	y_n	ϵ_c	ω_t	M_{th}	M_{th}		M_{th}	
(kips)	(in)	(in-kips)	(deg.)	(in)	(in)	(in)	(in/in x 10 ⁻⁴)	(in-kips)	(in-kips)	(in-kips)	(%)	(in-kips)	(%)
0	20.00	0	0	0.840	0	0	0	0	0	0	-	0	-
0.185	19.90	3.68	0.4	0.830	19.2	22.1	19.2	22.1	3.79	3	5.20	-10	
0.29	19.86	5.72	0.7	0.835	30.1	35.1	30.1	35.1	6.18	8	5.73	-7	
0.31	19.86	6.12	0.8	0.830	1.075	38.0	32.5	38.0	6.65	9	6.22	-5	
0.33	19.84	6.53	0.9	0.830	1.075	40.8	34.9	40.8	7.11	9	6.95	-6	
0.37	19.82	7.34	1.0	0.835	1.078	46.0	39.4	46.0	7.84	7	7.70	-5	
0.41	19.78	8.12	1.4	0.830	1.088	51.5	44.5	51.5	8.53	5	8.72	-8	
0.475	19.70	9.40	2.0	0.815	1.099	61.5	54.4	61.5	9.60	2	8.91	-10	
0.50	19.67	9.80	2.1	0.815	1.095	65.5	58.0	65.5	9.96	2	9.33	-10	
0.52	19.63	10.23	2.5	0.815	1.108	70.9	63.0	70.9	10.37	1	9.65	-12	
0.54	19.58	10.60	2.8	0.815	1.104	75.5	67.1	75.5	10.70	1	10.04	-13	
0.565	19.53	11.00	3.0	0.815	1.110	83.0	74.4	83.0	11.22	2	10.38	-13	
0.585	19.47	11.38	3.6	0.800	1.110	91.0	82.0	91.0	11.65	2	10.90	-12	
0.61	19.38	11.80	4.4	0.800	1.113	103	93.6	103	12.16	3	11.43	-10	
0.63	19.28	12.18	5.5	0.790	1.118	118	109	118	12.67	4			

^a From graphical solution assuming linear variation of strain.
 $M_{th}^n = \frac{I_c}{c_c} \frac{1}{\cos \theta} \left[f_{mc}^n + f_{oc}^n (k_c - 1) \right] = 0.0852 (f_{mc}^n + 0.667 f_{oc}^n)$

^b Resisting moment of compression and tension areas computed separately by Cosson's method assuming neutral axis stationary:

$M_{th}^c = \frac{I_c}{c_c} \frac{1}{\cos \theta} \left[f_{mc}^c + f_{oc}^c (k_c - 1) \right] = 0.081 (f_{mc}^c + 0.890 f_{oc}^c)$

^c Exponential equation: $M_{th} = \frac{21700}{k_c - 1} \rho$
^d Theoretical value.

^e Counterclockwise, referred to Figure 1.

Table No. 3 - LOAD AND STRAIN DATA
 Angle Beam H-L
 $\theta = 0^\circ$

Total load P (kips)	Mon. arm L (in)	Expt. bend. mom. M_t (in-kips)	Measured strains						
			ϵ_1 (+)	ϵ_2 (-)	ϵ_3 (+)	ϵ_4 (+)	ϵ_5 (-)	ϵ_6 (-)	ϵ_7 (+)
(in/in $\times 10^{-4}$)									
0	20.00	0	0	0	0	0	0	0	0
0.315	19.85	6.21	3.1	27.4	28.5	23.0	14.9	13.6	7.8
0.435	19.75	8.56	4.2	39.9	41.6	32.0	21.5	20.4	10.4
0.50	19.67	9.81	4.0	47.8	50.2	38.5	25.7	25.1	12.1
0.545	19.60	10.72	4.0	56.4	59.4	45.4	29.6	29.5	14.4
0.59	19.48	11.45	3.5	66.3	70.3	53.2	34.7	35.2	16.9
0.60	19.43	11.63	3.7	69.8	74.2	55.3	36.4	37.0	17.5
0.615	19.37	11.90	3.3	75.4	80.0	59.8	39.0	39.8	19.0
0.625	19.32	12.12	3.1	80.4	86.0	64.2	41.9	43.0	20.2
0.635	19.25	12.23	3.4	83.5	89.0	66.0	43.5	44.6	20.7
0.645	19.22	12.38	3.0	87.9	94.0	69.6	45.3	46.9	21.8
0.655	19.13	12.57	2.4	94.6	102	75.2	48.6	50.7	23.4
0.67	19.08	12.79	1.8	103	111	81.0	52.3	55.5	24.8
0.675	19.00	12.87	1.2	111	119	86.0	55.8	59.6	26.2
0.685	18.88	12.96	0	117	126	90.8	58.7	63.4	27.2
0.695	18.75	13.03	-2.0	128	139	98.2	63.0	70.1	28.5

Table No. 4 - THEORETICAL BENDING MOMENT
Angle Beam N-4
 $\theta = 0^\circ$

Expt. bend. mom.	Rotation (deg.)	Neutral axis location	Outer fiber strain	Compression area		Tension area		Theoret. bending moment (Cozz.)	Radius of curvature ρ	Theoret. bending moment (Expon.)			
M_t	(in-kips)	x_n (in)	y_n (in)	ϵ_c	ϵ_t	f_{mc} (ksi)	f_{oc} (ksi)	M_{th}^c (in-kips)	f_{mt} (ksi)	f_{ot} (ksi)	M_{th}^t (in-kips)	ρ	M_{th} (in-kips)
0	0	0.840	1.100	0	0	0	0	0	0	0	0	-	0
6.21	0.7	0.860	1.075	32.9	37.5	31.50	3.00	2.79	36.6	7.3	3.53	204	5.78
8.56	1.4	0.850	1.105	48.0	52.8	41.05	14.30	4.36	42.6	15.5	4.50	140	8.01
9.81	1.9	0.850	1.110	58.0	64.0	44.0	18.0	4.86	45.3	20.5	5.02	116	8.92
10.72	-	0.840	1.110	68.0	75.5	46.0	22.0	5.31	47.0	24.8	5.42	98.5	9.75
11.45	3.3	0.825	1.110	80.0	88.0	47.6	26.5	5.76	48.4	29.8	5.75	83.8	10.25
11.63	3.7	0.810	1.110	85.3	91.6	48.1	28.0	5.91	48.7	29.5	5.82	78.5	10.55
11.90	4.0	0.810	1.110	92.5	99.0	48.8	29.8	6.10	49.4	31.1	5.96	72.5	10.80
12.12	4.5	0.810	1.110	98.0	106.8	49.2	30.9	6.21	50.0	32.5	6.10	68.3	11.05
12.23	4.8	0.808	1.120	102.2	109.5	49.8	32.0	6.35	50.2	32.8	6.13	65.5	11.22
12.38	5.2	0.808	1.115	107.2	115.5	50.0	32.5	6.39	50.6	33.7	6.22	62.5	11.39
12.57	5.8	0.800	1.110	116.0	125.5	50.6	33.8	6.53	51.3	35.0	6.36	57.8	11.59
12.79	6.5	0.795	1.110	126	135	51.3	35.0	6.66	51.9	36.0	6.46	45.8	12.30
12.87	7.0	0.790	1.120	136	144	52.0	36.1	6.72	52.4	36.8	6.55	42.4	12.55
12.96	7.5	0.785	1.130	143	152	52.4	37.0	6.90	52.8	37.7	6.64	40.3	12.72
13.03	8.6	0.775	1.120	157	165	53.2	38.1	7.05	53.6	38.8	6.76	36.7	12.90

^a From graphical solution assuming linear variation of strain.

^b Resisting moment of compression and tension areas computed separately by Cozzone's method assuming neutral axis stationary:

$$M_{th}^c = \frac{I_c}{c_c} \frac{1}{\cos \theta} [f_{mc} + f_{oc} (k_c - 1)] = 0.081 (f_{mc} + 0.890 f_{oc})$$

$$M_{th}^t = \frac{I_t}{c_t} \frac{1}{\cos \theta} [f_{mt} + f_{ot} (k_t - 1)] = 0.0852 (f_{mt} + 0.667 f_{ot})$$

$$M_{th} = M_{th}^c + M_{th}^t$$

^c Exponential equation: $M_{th} = \frac{21700}{n-1} \rho$
^d Theoretical value.

^e Counterclockwise, referred to Figure 1.

Table No. 5 - COMPARISON OF THEORETICAL AND
EXPERIMENTAL BENDING MOMENTS
Angle Beam M-4
 $\theta = 0^\circ$

Expt. bend. mom.	Cossons's Method			Exponential Method		
	M_t (in-kips)	M_{th} (in-kips)	ratio M_{th}/M_t	diff. (%)	M_{th} (in-kips)	ratio M_{th}/M_t
0	0	-	-	0	-	-
6.21	6.32	1.017	2	5.78	0.930	-7
8.56	8.86	1.035	4	8.01	0.936	-6
9.81	9.88	1.005	0	8.92	0.909	-9
10.72	10.73	1.000	0	9.75	0.910	-9
11.45	11.51	1.007	1	10.25	0.895	-11
11.63	11.73	1.008	1	10.55	0.907	-9
11.90	12.06	1.012	1	10.80	0.907	-9
12.12	12.31	1.016	2	11.05	0.912	-9
12.23	12.48	1.020	2	11.22	0.918	-8
12.38	12.61	1.020	2	11.39	0.920	-8
12.57	12.89	1.024	2	11.59	0.923	-8
12.79	13.12	1.028	3	12.30	0.963	-4
12.87	13.28	1.032	3	12.55	0.977	-2
12.96	13.54	1.045	4	12.72	0.982	-2
13.03	13.81	1.060	6	12.90	0.990	-1

Table No. 6 - TEST RESULTS
 Angle Beta $\beta = 5^\circ$
 $\theta = 60^\circ$

Total load	Mom. arm	Expt. bend. mom.	Notation	Neutral axis location	Outer fiber strain	Theoret. bending moment (Cosz.)	Diff. (Cosz.)	Theoret. bending moment (Expon.)	Diff. (Expon.)
P (kips)	L (in)	M_t (in-kips)	(deg.)	x_n (in)	y_n (in)	ϵ_c (in/in $\times 10^{-4}$)	(%)	M_{th} (in-kips)	(%)
SECTION A									
0	20.60	0	0	0.476	1.686	0	0	0	-
0.07	19.81	1.38	0.1	0.490	1.730	19.0	15	1.58	-
0.14	19.47	2.74	0.4	0.482	1.700	37.8	14	2.90	6
0.20	19.05	3.84	0.5	0.471	1.735	58.1	8	3.91	2
0.22	18.80	4.18	0.6	0.463	1.770	67.5	6	4.16	0
0.245	18.44	4.55	0.7	0.454	1.815	79.5	4	4.44	-3
0.28	17.80	4.94	1.0	0.440	1.840	97.5	4	4.79	-3
0.30	17.40	5.20	1.3	0.435	1.855	110	2	4.95	-4
0.325	16.70	5.45	1.6	0.425	1.880	127	1	5.15	-6
0.355	15.80	5.61	2.3	0.419	1.900	144	1	5.30	-6
0.38	15.40	5.83	2.5	0.416	1.910	152	-2	5.40	-8
SECTION B									
0.07	19.88	1.38		0.485	1.660	19.0	17	1.62	-
0.14	19.50	2.74		0.485	1.690	37.5	14	3.12	6
0.20	19.12	3.85		0.475	1.720	57.6	7	3.96	3
0.22	18.90	4.20		0.465	1.775	66.4	6	4.20	0
0.245	18.53	4.57		0.455	1.785	79.0	4	4.50	-2
0.28	17.90	4.97		0.438	1.830	97.5	3	4.86	-2
0.30	17.58	5.25		0.432	1.855	110	1	5.02	-4
0.325	16.84	5.49		0.422	1.870	129	0	5.20	-5
0.355	16.00	5.68		0.416	1.880	148	0	5.45	-4
0.38	15.55	5.89		0.412	1.900	157	-2	5.55	-6

Table No. 6 - (Continued)

Total load (kips)	Mem. arm (in)	Expt. bend. mom.	Neutral axis location (in)	x_n (in)	y_n (in)	e_c (in/in $\times 10^{-4}$)	Outer fiber strain ϵ_t	Theoret. bending moment (Cosz.) M_{th} (in-kips)	Diff. (Cosz.) (%)	Theoret. bending moment (Expon.) M_{th} (in-kips)	Diff. (Expon.) (%)
0.07	19.90	1.39	0.492	1.710	18.0	24.7	1.49	7	2.88	-5	
0.14	19.60	2.75	0.485	1.710	36.8	50.5	3.03	10	3.92	1	
0.20	19.30	3.89	0.480	1.710	56.5	79.5	4.04	4	4.20	-1	
0.22	19.10	4.25	0.465	1.770	66.4	95.5	4.42	4	4.50	-3	
0.245	18.80	4.63	0.455	1.805	79.0	120	4.76	3	4.87	-4	
0.28	18.22	5.05	0.440	1.855	98.5	158	5.13	2	5.08	-5	
0.30	17.95	5.36	0.431	1.880	113	188	5.34	0	5.32	-6	
0.325	17.35	5.65	0.420	1.890	136	232	5.58	-1	5.50	-6	
0.355	16.59	5.98	0.412	1.915	159	281	5.78	-2			

SECTION C

^aFrom graphical solution assuming linear variation of strain. $M'_{th} = \frac{I_t}{c_t} \frac{1}{\cos \phi} [f_{mt} + f_{ot} (k_t - 1)] = 0.0319 (f_{mc} + 0.840 f_{oc})$

^bResisting moment of compression and tension areas computed separately by Cosson's method assuming neutral axis stationary: $M'_{th} = M'_{th} + M''_{th}$

$$M'_{th} = \frac{I_c}{c_c} \frac{1}{\cos \phi} [f_{mc} + f_{oc} (k_c - 1)] = 0.0316 (f_{mc} + 0.865 f_{oc})$$

$$M''_{th} = \frac{9100}{p^{n-1}} - 17.70 \rho$$

^dTheoretical value.

^eCounterclockwise, referred to Figure 1.

Table No. 7 - TEST RESULTS
Angle Beam N-6
 $\theta = 300$

Total load (kips)	Mon. arm L (in)	Expt. bend. mom. M_t (in-kips)	^e Rotation (deg.)	^a Neutral axis location x_n (in)	y_n (in)	e_c (in/in $\times 10^{-4}$)	^e t fiber strain	^b Theoret. bending moment (Cons.) M_{th} (in-kips)	Diff. (Cons.) (%)	^c Theoret. bending moment (Expon.) M_{th} (in-kips)	Diff. (Expon.) (%)
0	20.00	0	0	0.513	1.466	0	0	0	-	0	-
0.06	19.92	1.23	0	0.530	1.480	12.6	15.0	1.29	4	0	-
0.125	19.76	2.46	0.2	0.540	1.470	26.0	29.0	2.66	6	0	-
0.18	19.63	3.62	0.5	0.535	1.460	37.7	43.0	3.96	9	3.57	-1
0.245	19.48	4.80	0.8	0.535	1.450	50.5	56.0	4.88	2	4.60	-4
0.31	19.17	5.90	1.5	0.535	1.482	70.8	78.0	5.49	-7	5.45	-8
0.345	18.87	6.53	2.2	0.523	1.515	91.5	105	6.16	-5	6.06	-7
0.39	18.38	7.18	3.8	0.512	1.540	122	147	7.23	1	6.65	-7
0.43	17.69	7.60	6.0	0.485	1.565	161	198	7.73	4	7.12	-6
0.47	16.70	7.88	9.0	0.475	1.585	200	269	8.14	3	7.42	-6
0.50	16.46	8.04	10.5	0.475	1.540	220	306	8.30	3	7.60	-6

^aFrom graphical solution assuming linear variation of strain.

^bResisting moment of compression and tension areas computed separately by Coszone's method assuming neutral axis stationary:

$$M'_{th} = \frac{I_c}{c_c} \frac{1}{\cos \theta} \left[f_{mc} + f_{oc} (k_c - 1) \right] = 0.0427 (f_{mc} + 0.930 f_{oc})$$

$$M''_{th} = \frac{I_t}{c_t} \frac{1}{\cos \theta} \left[f_{mt} + f_{ot} (k_c - 1) \right] = 0.0434 (f_{mt} + 0.863 f_{ot})$$

$$M_{th} = M'_{th} + M''_{th}$$

$$M_{th} = \frac{17,000}{p} - 22.33 p$$

^cTheoretical value.

^eCounterclockwise, referred to Figure 1.

Table No. 8 - TEST RESULTS
 Angle Beam N-7
 $\theta = 76^\circ 7'$

Total load (kips)	Non. arm (in)	Expt. bend. mom. (in-kips)	Rotation (deg.)	Neutral axis location (in)	x_n (in)	y_n (in)	ϵ_c (in/in $\times 10^{-4}$)	ϵ_t	Theoret. bending moment (Coss.) (in-kips)	Diff. (Coss.) (%)	Theoret. bending moment (Expon.) (in-kips)	Diff. (Expon.) (%)
P	L	M_t			x_n	y_n	ϵ_c	ϵ_t	M_{th}		M_{th}	
0	20.00	0	0	0.449	0.449	1.815	0	0	0	-	0	-
0.55	19.77	1.08	0	0.449	0.449	1.812	13.8	20.2	1.15	6	1.66	-18
0.10	19.50	1.96	0	0.449	0.449	1.822	24.5	39.0	2.14	9	2.60	3
0.13	19.31	2.52	0.2	0.445	0.445	1.830	33.3	53.0	2.82	12	3.26	9
0.16	19.09	2.95	0.5	0.433	0.433	1.851	42.0	68.8	3.32	11	3.61	11
0.17	18.89	3.22	0.2	0.425	0.425	1.879	49.0	82.0	3.71	13	3.90	12
0.18	18.69	3.42	0.2	0.418	0.418	1.900	55.2	93.5	3.94	13	4.20	13
0.20	18.44	3.65	0.2	0.410	0.410	2.933	62.8	112	4.20	13	4.46	12
0.215	18.05	3.90	0	0.400	0.400	1.962	72.4	132	4.46	12	4.75	13
0.235	17.61	4.13	0	0.392	0.392	1.991	82.5	159	4.68	12	4.90	13
0.25	17.19	4.28	0	0.383	0.383	2.013	91.0	179	4.84	12	5.04	12
0.265	16.70	4.45	0	0.379	0.379	2.036	99.8	200	4.97	11	5.18	12
0.28	16.19	4.57	0	0.375	0.375	2.049	109	224	5.07	10	5.30	12
0.305	15.45	4.73	0	0.371	0.371	2.061	119	251	5.20	9		11

^aFrom graphical solution assuming linear variation of strain.
 $M_{th}'' = \frac{I_c}{c_c} \frac{1}{\cos \beta} [f_{mc} + f_{ot}(k_c - 1)] = 0.031(f_{mc} + 0.790 f_{ot})$

^bResisting moment of compression and tension areas computed separately by Cossone's method assuming neutral axis stationary:
 $M_{th}' = \frac{I_c}{c_c} \frac{1}{\cos \beta} [f_{mc} + f_{oc}(k_c - 1)] = 0.029(f_{mc} + 0.892 f_{oc})$

^cExponential equation: $M_{th} = \frac{8536}{P^{B-1}} - 19.46 P$
^dTheoretical value.

^eCounterclockwise, referred to Figure 1.